Validation of a 1/20th Scaled VHTR Far-Field Air/Helium Mixing Apparatus

A Thesis

Presented in Partial Fulfillment of the Requirements for the

Degree of Master of Science

with a

Major in Nuclear Engineering

in the

College of Graduate Studies

University of Idaho

by

Joseph Hafen

Major Professor: Richard Christensen, Ph.D.

Committee Members: Michael McKellar, Ph.D.; David Arcilesi, Ph.D.

Department Administrator: Indrajit Charit, Ph. D.

May 2021

Authorization to Submit Thesis

This thesis of Joseph Hafen, submitted for the degree of Master of Science with a major in Nuclear Engineering and titled "Validation of a 1/20th Scaled VHTR Far-Field Air/Helium Mixing Apparatus," has been reviewed in final form. Permission, as indicated by the signatures and dates given below, is now granted to submit final copies to the College of Graduate Studies for approval.

Major Professor: _____Date_____
Richard Christensen, Ph.D.

Committee Members: _____Date_____
Michael McKellar, Ph.D.

_____Date_____
David Arcilesi, Ph.D.

Department Administrator: _____Date_____
Indrajit Charit, Ph.D.

Abstract

The Very High Temperature Reactor (VHTR) is a promising Gen-IV reactor design. It is a helium cooled reactor capable of heating its coolant to 1000° C before it exits the reactor core. Such exit temperatures make it feasible to achieve a power output of 800 MWth. Its design is currently being researched by the United States Department of Energy (DOE).

One element of its design currently under investigation is the possibility of a failure at a fuel rod drive housing, or any other instrumental housing located on the reactor pressure vessel (RPV). A structural failure of the RPV would lead to a rapid depressurization of the reactor's pressurized loop and a loss of cooling accident (LOCA). If oxygen enters the reactor core following the LOCA, it could chemically react with the high temperature graphite in the reactor core, jeopardizing its structural integrity, and risking a release of radioactive contamination to the surrounding environment. One way of preventing air ingress into the reactor core is by understanding the mixing phenomena of helium and air in the containment structure surrounding the RPV. This thesis discusses the experimental and computational efforts performed at the University of Idaho to understand the helium/air mixing patterns inside the VHTR's containment structure following a LOCA.

Table of Contents

List of Tables

List of Figures

Nomenclature

$LOCA$	Loss of Cooling Accident
GFR	Gas-Cooled Fast Reactor
LFR	Lead-cooled Fast Reactor
MSR	Molten Salt Reactor
SFR	Sodium-cooled Fast Reactor
$VHTR$	Very High Temperature Reactor
$SCWR$	Super Critical Water-cooled Reactor
PWR	Pressurized Water Reactor
INL	Idaho National Laboratory
ANL	Argonne National Laboratory
$NGNP$	Next Generation Nuclear Plant
DCC	Depressurized Conduction Cooling
RPV	Reactor Pressure Vessel
PGV	Power Generation Vessel
$HTGR$	High Temperature Gas Reactor
c_p	specific heat
k	thermal conductivity

g	acceleration due to gravity
T_s	surface temperature
T_∞	bulk temperature
D	diameter
ν	kinematic viscosity
Re	Reynolds number
L	Length
u	velocity
$ASME$	American Standard of Mechanical Engineering
RTD	Resistance Temperature Detector
V_{He}	Volume of Pressurized Helium
V_{RPV}	Volume of the RPV
C	Conversion unit from cubic meters to cubic feet
$P_{pre-heat}$	Pressure of RPV
P_{atm}	effective width
N_R	Number of gas room replacements

Greek Symbols

β	coefficient of thermal expansion
η	dynamic viscosity

ρ	fluid density

Subscripts

∞	average temperature of a body of gas
atm	atmoshpheric
He	Helium
p	constant pressure
$pre-heat$	prior to heating the helium
RPV	RPV
s	surface
R	room replacement

CHAPTER 1

Introduction

1.1 Background

The six Generation-IV reactor designs currently under investigation by the United States Department of Energy (DOE) include the gas-cooled fast reactor (GFR), the lead-cooled reactor (LFR), the molten-salt reactor (MSR), the sodium-cooled fast reactor, the super critical water-cooled reactor (SCWR), and the Very High Temperature Reactor (VHTR). Research programs on these respective reactor designs have a common set of goals. These goals are to build a generation of nuclear reactors that are safer, longer lasting, proliferation-resistant and more economically viable than previous generations of nuclear reactors. [1]

The VHTR is a helium cooled reactor. It is estimated that this design will deliver exit coolant temperatures of 1000° C. [2] [3] Coolant exit temperatures in this range make it feasible to achieve power output of 800 MWth with a higher efficiency than Pressurized Water Reactors (PWR) and Boiling Water Reactors (BWR). [2] Its reactor pressure vessel (RPV) is nearly twice the size of the BWR's RPV. [1] The size and method of cooling the reactor core contribute to the high exit temperature.

This thesis discusses research performed at the University of Idaho to help accomplish the safety goals of the VHTR which inspired its design. It focuses on the helium/air mixing patterns following a Loss of Cooling Accident (LOCA) in a VHTR. A key element in the safety analysis of a VHTR is a depressurized loss of forced circulation followed by air ingress. This could happen as a result of a RPV structural failure at a fuel rod drive housing or any instrumentation housing on the RPV. A structural failure and rupture of the RPV leads to its rapid depressurization of high-pressure helium gas into the reactor cavity, which is filled with air during normal operation. As pressure

accumulates within the reactor cavity, this forces a helium gas/air mixture to exit the reactor cavity via a ventilation duct to the environment. The dynamics of the primary system depressurization in concert with the loss of air and helium gas from the reactor cavity set the initial conditions for the subsequent ingress flow into reactor pressure vessel. For example, the depressurization establishes the air and helium gas concentration near the break and throughout the reactor cavity at the onset of ingress flow. The depressurization also establishes the gas temperature near the break on the inside and outside of the RPV as well as throughout the reactor cavity and RPV at the onset of ingress flow. Both of the aforementioned factors have a significant impact on the rate at which air will ingress into the RPV and the amount of air that is available for ingress into the RPV. To understand the far-field effects of a VHTR depressurization following a small break LOCA event, it is proposed that a scaled VHTR reactor system be designed and constructed to perform high-temperature, high-pressure experiments to increase understanding of the depressurization phenomenology with a reactor cavity structure and its impact on the following stages of the small break LOCA event.

1.2 Literature Review

In 2010, the Idaho National Laboratory (INL), Argonne National Laboratory (ANL), and DOE published, "The Next Generation Nuclear Plant (NGNP) Methods Technical Program Plan." [4] This document discusses the challenges of incorporating the performance objectives of the Generation IV program reactors in the design and licensing application of a VHTR. The authors identified each major system of the VHTR and its individual components which merit research. Table 1.1 shows all of the systems and their individual components identified in their paper. It was determined that failure analysis be performed on each component of each system.

Table 1.1: A list of the VHTR systems and components under investigation. [4]

System	Component
Reactor Vessel	Inlet Plenum Riser Upper Plenum and Components Core Reflectors Lower Plenum and Components
Reactant Coolant Loop	Hot-Cold Loop
Power Conversion System (Direct Cycle)	Turbine Recuperator Precooler LP Compressor Intercooler HP Compressor
RCCS	Reactor Cavity (Confinement) RCCS Tube (Air Duct) RCCS Piping and Chimney
Intermediate Heat Exchange (IHX)	Primary Side Secondary Side
Shutdown Cooling System (SCS)	Pumps Coolers

Previous analysis identified the depressurized conduction cooling (DCC) failure event as an important research topic. [5] A DCC event occurs when a reactor is running at 100% power and a double-ended guillotine (DEGB) break occurs. A DEGB is a rupture at the hot and cold ducts between the RPV and Power Generation Vessel (PGV). This break initiates a blowdown event and a rapid depressurization of the reactor's pressurized loop. [6] Studying this event is important because a rapid depressurization of the reactor core can result in air ingress into the core. Oxygen ingress into the reactor core could result in oxidization in and damage to the reactor core, along with a release of carbon monoxide. [7]

Initially, it was assumed that a DCC event would consist of three sequential phases: the blowdown phase, the molecular diffusion phase, and the natural convection phase. Kim et al. [8] discussed these three phases later in 2008, and suggested that this list was

incomplete. Contrary to the previous assumption that molecular diffusion was the sole mechanism for air ingress, he stated that air ingress via density-driven stratified flow was a significant mechanism of air ingress. He also noted that density driven stratified flow was determined by different mechanisms at different times. [8] [9] He referred to an analysis by Oh et al. [10] which suggested that the stratified flow following a break in the VHTR could be a method of air entering the VHTR before molecular diffusion could occur.

Arcilesi performed further research on this topic at The Ohio State University by determining which mechanism of air-ingress dominated at initial stages of a blowdown event following a DEGB. [11] His data showed that during early stages of a blowdown event, the predominant air ingress mechanism was density-driven stratified flow.

Arcilesi's research at The Ohio State University confirmed prior research by Kim [9] and Oh [10], that density-driven stratified flow dominates air ingress at early stages of the blowdown. This discovery drastically changes previous assumptions of molecular diffusion being the sole driving air ingress mechanism. Density-driven stratified flow allows earlier onset of natural circulation within the core. It also results in more rapid oxidation in the reactor core. [12]

Arcilesi confirmed the importance of understanding both types of air-ingress mechanisms by explaining that they could be important at different times for different scenarios. [8], [12] Arcilesi's research scope included the thermal-hydraulic behavior following a break in the hot duct and hot exit plenum. He suggested that future research evaluate breaks at different sizes, orientations, shapes and locations. In order to better understand air-ingress phenomena, Arcilesi included in future work suggestions research of in-vessel components such as the core, upper and lower plenum, and the cold duct of the co-axial cross vessel. He also suggested that his research would advance future understanding of the transition from natural circulation within the hot plenum to global natural circulation

with the RPV. [11]

His future work suggestions align with the initial research discussed in Table 1.1. The focus of the research presented in this thesis is to demonstrate the ability of the apparatus constructed at the University of Idaho to model helium/air mixing patterns following a LOCA of a VHTR and give insight on how to improve it for future experimentation. The research performed at the University of Idaho is a collaborative effort with the University of Michigan with an end goal of understanding all mechanisms contributing to air-ingress into the reactor following a LOCA. [11] Blowdown phenomena and mixing patterns following a LOCA are major indicators of potential oxygen ingress via molecular diffusion. This thesis aims to explain the blowdown phenomena to increase understanding of air ingress.

1.3 Motivation

The helium cooled VHTR currently under investigation is designed to heat helium to approximately 1000° C before it exits the RPV. [3] It is estimated to produce up to 800 MWth. However, serious consequences are associated with a LOCA. These risks include the possibility or releasing radioactive waste into the environment or jeopardizing the structural integrity in the reactor core. The motivation behind the research presented in this thesis is to increase the safety of this nuclear reactor design by understanding the patterns of helium/air mixing following a LOCA. This understanding of gas mixing patterns will lead to a greater understanding of how to mitigate risks associated to a LOCA.

1.4 Goal

This project has multiple goals. The first goal is to construct an apparatus capable of mimicking the gas mixing patterns in the full VHTR. The second goal is to obtain data describing helium and air mix patterns following a rapid depressurization of the reactor core. The data acquired in this process will be used to validate codes to determine optimal methods of venting the VHTR system. Effectively venting the VHTR system will minimize oxygen ingress into the RPV during a LOCA. This thesis discusses work done to achieve the first goal by demonstrating the progress made in developing a scaled VHTR system and its ability to accurately mimic a blowdown of the prototype.

1.5 Approach

This goal was achieved by experimental and computational means. Preliminary blowdowns were performed with a 1/20th scaled VHTR apparatus to demonstrate its effectiveness and provide insights to how the model could be improved. This apparatus design includes a pressurized vessel representing the RPV, a larger non-pressurized vessel representing the PGV, a containment structure designed for each vessel, and a co-axial cross vessel connecting the RPV and PGV containment structures. The carbon steel containment structure surrounding the two vessels represents the concrete containment that will surround the RPV and PGV. There are seven blowdown ports on the RPV capable of mimicking the flow patterns of helium escaping the containment during the LOCA events. Eleven windows are built onto the containment structure. These windows house instrumentation which enable blowdowns of the pressurized vessel and ventilation for the containment. This instrumentation is discussed later in the thesis. During the blowdown, all windows will be closed except one window to ventilate the containment structure.

Computational Fluid Dynamics (CFD) analysis was performed in StarCCM++ and

analytical solutions were performed with Python. Computational data aids in instrumentation placement inside the apparatus and improves the project's procedures.

1.6 Thesis Outline

Chapter two discusses the project and apparatus design. It includes the governing equations to maintain thermal hydraulic similarity between the apparatus and the prototype. These governing equations identify the flow regime and the number of times the air in the containment will be replaced by the helium in the RPV in the prototype and the apparatus.

Chapter three discusses the design of all components for the apparatus including the vessels, the containment structures, the blowdown ports, the ventilation port, preliminary tests, and all instrumentation. It describes the apparatus design. This includes the dimensions and metal types of the vessels and their containment structures. It discusses instrumentation housing including the cooling tube manifold instrumentation, the ventilation port instrumentation, the pneumatic ram, and all other instrumentation included in the apparatus. It also discusses instrumentation calibration. The methods for CFD analysis and the CFD results are discussed at the end of this section.

Chapter four discusses the tests and results used to demonstrate the facilities ability to study helium/air mixing patterns following the blowdown. It presents parameters and results from three preliminary blowdown tests. The effectiveness of the instrumentation is discussed.

Chapter five shows the two methods of predictive modelling prior to experimentation. A computational fluid dynamics (CFD) simulation is performed using StarCCM+ to determine the gas patterns inside the containment following the LOCA. The second method of predictive modelling is an analytical solution. It predicts the blowdown time

of the system into ambient room temperatures with no containment structure.

Chapter six gives conclusions and suggests the future work. It duscusses the system's effectiveness in determining helium/air mixing patterns. It discusses areas that the equipment failed or succeeded to obtain accurate data. Consistent phenomena during the blowdowns is identified. Finally, future works and research focuses are suggested.

CHAPTER 2

Project Design

2.1 Preliminary Research Summary

At the early stages of this project, it was decided that a $\frac{1}{20}$th scaled model, or apparatus, would be constructed to model a blowdown event in a full scaled VHTR, or prototype. This decision was determined based on space, budgetary, and fabrication considerations. In order to maintain thermal hydraulic similarity between the apparatus and the prototype, the apparatus's Reynolds number at the locations of greatest flow restriction needed to match those of the prototype. The apparatus also needed to match the prototype in the number of gas-volume replacements that would occur in the containment structure as a result of the blowdown. Given the size of the apparatus, preliminary calculations suggested that the Reynolds number and volume replacements in each system would match with initial conditions of 250 psig and 250°. The methodology is explained in the rest of this chapter.

2.2 Governing Equations for Thermal Hydraulic Similarity

This section discusses the thermal hydraulic similarity between the $\frac{1}{20}$th scaled apparatus and the prototype during the blowdown phase. The blowdown phase is characterized by three sequential stages: forced convection, mixing, and stratification. The forced convection's driving force is provided by the helium gas rapidly evacuating the RPV and expanding in the RPV's containment structure. Forced convection causes the helium and air gases to mix. It is assumed that at time scales longer than the blowdown's time scale, the gases will separate via molecular diffusion due to the difference of gas densities. The helium mass flow rate values will be significantly higher at the initial stages of the blowdown, and the majority of the helium's rapid release and rapid expansion occurs in

initial stages of the blowdown. Based on expected blowdown time scales and molecular diffusion time scales, the majority of the blowdown is expected to occur before molecular diffusion occurs. This thesis focuses on the blowdown phase and the apparatus's ability to mimic and record the blowdown phenomena.

Two comparisons were made between the apparatus and the prototype to maintain thermal hydraulic similarity during the blowdown phase. First, calculations were performed to determine the volume that the pressurized and heated helium gas in the RPV would occupy when cooled and expanded to standard atmospheric pressure and temperature. The volume that the helium would occupy, after being expanded and cooled, was compared to the volume between the RPV, PGV, and containment structure. This calculation ensures that the gas-volume changes occurring in the containment structure resulting from the blowdown are the same in each system. Second, the Reynold's numbers were compared at the two locations of greatest restriction in each system. The location of greatest restriction in each system is the blowdown port. The second most restrictive area is the ventilation port. These locations are determined by their cross-sectional areas, and not their hydraulic diameters. The size of the ventilation port in the prototype is unknown, and is not included in this thesis. A suggested size for the prototype's blowdown port is included later to maintain the Reynolds number at the ventilation port.

The Reynolds number is determined by Equation 2.1:

$$\mathrm{Re} = \frac{\rho u L}{\mu} \tag{2.1}$$

where ρ is the density of the gas exiting the pressure vessel, u is the exit temperature, L is the characteristic length, or the hydraulic diameter of the blowdown orifice, and μ is the dynamic viscosity.

The gas-volume replacement calculation is performed with equation 2.2:

$$N_R = \frac{V_{He}}{V_{cont}} \tag{2.2}$$

where N_R is the number of times the gas in the entire containment can be replaced by the blowdown of the pressure vessel, V_{He} is the volume of gas the helium would occupy if it were at standard pressure and temperature, and V_{cont} is the volume of the RPV containment structure minus the volume of the RPV.

2.2.1 Prototype Thermal Hydraulic Calculations

The values used to calculate the prototype's Reynolds number and the number of times the gas in the entire containment can be replaced by the blowdown are shown in Table 2.1 and Table 2.2. [13] Table 2.1 contains gas constants, blowdown geometries, and the choke flow velocity for gas exiting the RPV.

Table 2.1: Values used to calculate the Reynolds numbers of the prototype

Variable	Value	Units
c_p	5192.6	$\frac{J}{KgK}$
μ	5.01e-5	Pa * s
k	0.23	$\frac{kg*m}{K*s^2}$
g	9.8	$\frac{m}{s^2}$
β	8.9e-4	$\frac{1}{K}$
T_s	1123	K
T_∞	365	K
D	23.7	m
ρ	3.001	$\frac{kg}{m^3}$
L	0.009652	m
u	1007	$\frac{m}{s}$

The Gas-Turbine Modular Helium Reactor (GT-MHR) Conceptual Design Description Report [13] provides the temperatures of the helium coolant entering and exiting the reactor core, the pressure of the reactor loop, and the dimensions of the RPV, PGV, and

the containment structure. The dimensions, pressure, and temperatures of the GT-MHR are found in Table 2.2. The pressurized coolant volume also includes an estimation of the coolant in the PGV. The volume of the pressurized loop in the PGV was determined by taking an average value of different cross flow sections in the PGV and its height.

Table 2.2: Dimensions, temperatures, and pressures of the GT-MHR.

Dimension/Property	Value	Units
Inlet Temperature	751	K
Exit Temperature	1123	K
Pressure	1003	psia
RPV Diameter	27.5	feet
PGV Diameter	27.93	feet
PGV and RV Containment Side Length	102	feet
H	140	feet

Table 2.3 shows the dimensionless parameters calculated using the values in Tables 2.1 and 2.2.

Table 2.3: Prototype Dimensionless Parameters

Dimension	Value	Units
Blowdown Port Reynolds number	$5.82 * 10^5$	Dimensionless
Ventilation Port Reynolds number	//	Dimensionless
N_R	3.80	Dimensionless

2.2.2 Scaled Reactor Thermal Hydraulic Calculations

Tables 2.4 and 2.5 show the test parameters, variables, and dimensions of the apparatus determined during the initial design phases of this project. The scaled system's initial conditions are 250° C and 250 psig. The variables in these tables contain are used to determine the Reynolds number in Equation 2.1. Table 2.4 contains gas constants, blowdown geometries, and the choke flow velocity for gas exiting the RPV.

Table 2.4: Values used to calculate the apparatus Reynolds number.

Variable	Value	Units
c_p	5192.6	$\frac{J}{KgK}$
μ	2.592e-5	Pa * s
k	0.23	$\frac{kg*m}{K*s^2}$
g	9.8	$\frac{m}{s^2}$
β	0.0019	$\frac{1}{K}$
T_s	523	K
T_∞	398	K
D	1.346	m
ν	1.85e-5	$\frac{m^2}{s}$
ρ	1.68	$\frac{kg}{m^2}$
L	0.009652	m
u	1188.4	$\frac{m}{s}$

Table 2.5 shows the dimensions, temperature, and pressure of the apparatus to perform its gas-volume replacement calculation. Table 2.6 shows the dimensionless parameters calculated using the values in Tables 2.4 and 2.5.

Table 2.5: Apparatus Dimensions, temperatures, and pressures.

Dimension	Value	Units
Temperature	523	K
Pressure	264	psia
RPV Diameter	16	inches
PGV Diameter	16	inches
Containment Side Length	20.5	inches
Containment Height (RPV + PGV)	124.64	inches
Height	50.35	inches
L_{avg}	13.18	inches

Table 2.6: Apparatus Thermal Hydraulic Comparison Values

Dimension/Property	Value	Units
Blowdown Port Re	$7.02 * 10^5$	Dimensionless
Ventilation Port Re	$2.45 * 10^6$	Dimensionless
N_R	3.85	Dimensionless

2.2.3 Thermal Hydraulic Comparisons

Table 2.7 compares the Reynolds number and the number of gas room transfers in the apparatus and the prototype.

Table 2.7: Thermal Hydraulic Comparisons

	Prototype	Apparatus
Blowdown Port Reynolds number	$5.82 * 10^5$	$7.02 * 10^5$
Ventilation Port Reynolds number	//	$2.56 * 10^6$
N_R	3.80	3.85

The blowdown port Reynolds number in the apparatus is 20% larger than the blowdown port Reynolds number in the prototype. They both are categorized as turbulent flow according to Equations 2.3 - 2.5. The apparatus's ventilation port Reynolds number value is $2.56 * 10^6$. The prototype's ventilation port Reynolds number is not given because the cross sectional area and hydraulic diameter are not known. To make the Reynold's number match at the ventilation ports on the prototype and scaled system, an appropriate ventilation port for the prototype would have a height of 1.3 meters and a length of 3.25 meters. The gas-volume replacement calculations have negligible error.

$$\text{Laminar Flow: } Re < 2300 \tag{2.3}$$

$$\text{Transitional Flow: } 2300 < Re < 4000 \tag{2.4}$$

$$\text{Turbulent Flow: } 4000 < Re \tag{2.5}$$

2.3 Thermal Hydraulic Conclusions

These thermal hydraulic calculations and comparisons attempt to describe the VHTR blowdown phenomenology within a reactor cavity structure and maintain similarity between the two systems. By designing the apparatus in a way that conserves the Reynolds

number at the blowdown and ventilation port with the prototype, the turbulence flow patterns are also conserved in each system. Maintaining turbulence flow in the prototype and scaled system suggests that each system will demonstrate similar forced convection, mixing, and stratification patterns. Within the brief blowdown time scale following a small break LOCA, depressurization of the primary system is the dominant phenomenology until the fluid pressure within the RPV and the containment structure approaches one atmosphere. For this reason, the blowdown phenomenology does not immediately impact the oxygen ingress into the RPV. It does, however, establish the initial conditions for any air ingress scenario or subsequent phenomena. By maintaining thermal hydraulic similarity, the subsequent phenomena will be more similar due to matching Reynolds numbers and room replacement values.

This thesis does not discuss phenomenology past the blowdown phase. It demonstrates the apparatus's ability to mimic a blowdown similar to a prototypic blowdown and acquire data that accurately depicts the blowdown's gas flow phenomenology.

CHAPTER 3

Experimental Procedures, Materials, and Methods

3.1 Apparatus Design

A $\frac{1}{20}$th scale model of a VHTR was designed and fabricated to facilitate the analysis of a DCC and LOCA event. The model includes the following key components: the RPV and PGV, a co-axial cross vessel between the RPV and PGV, the containment vessel and a map of instrumentation. This section uses sketches made in SolidWorks and real images to illustrate the design and construction of the apparatus. Figure 3.1 shows the finished apparatus designed to understand helium/air mixing patterns inside following a rapid depressurization of a VHTR reactor core. The overall system design and original CAD drawings were completed by Jason Palmer, at the University of Idaho. The author specified, calibrated, wired, and attached all instrumentation to the apparatus. The author also oversaw the complete construction and proof testing of the apparatus and modified many dimensions of the apparatus which enabled them to function properly.

3.1.1 Scaled Reactor Pressure Vessel

The apparatus is capable of mimicking the helium-air mixing patterns in a VHTR following a loss of coolant accident by permitting a rapid depressurization from a pressurized ASME stamped pressure vessel surrounded by a containment. The gas mixing patterns in the experimental setup mimic the actual gas mixing patterns because the experimental setup maintains thermal-hydraulic similarity to the full scale model. The apparatus contains six blowdown ports varying vertically and radially around the pressure vessel, making it capable of performing experiments at each different location. Each location allows blowdown events to be initiated with different sizes of breaks. The containment allows ventilation options at eleven different locations between the structure outside of the

Figure 3.1: The assembled $\frac{1}{20}$th scaled model of a VHTR.

pressurized reactor vessel and power generation vessel.

The ASME stamped pressure vessel was fabricated by Buckeye Fabricating, in Springboro, OH. It is made of a 16-inch outer diameter schedule-40 stainless steel-316. On the top are nine entry ports with Swagelok fittings to fasten 3/4 inch heating cartridges into the ports. Image 3.2a shows the reactor pressure vessel's two sides where blowdowns can be initiated. Figure 3.2b shows heating cartridge ports at the top of the pressure vessel. The heating cartridges are fastened to the pressure vessel by swagelok fittings.

The RPV was designed to perform experiments at 250 psig. The pressure vessel was tested and rated for use up to 435 psig with a hydrostatic pressure test. The vessel was rated at 1000° F. The data sheet also specifies that the minimum temperature for the RPV is -20 ° F. There is no tolerance for corrosion, indicating that it is not fit for for any reacting chemical . [14]

Reactor Vessel Blowdown Port

As stated before, the reactor pressure vessel contains six different locations where blowdowns can be initiated. The ports were created individually from the rest of the reactor pressure vessel and then welded onto the reactor pressure vessel. They are 2.63 inches in diameter and 1.44 inches tall, similar to the shape of a hockey puck. The Solidworks sketch of the blowdown port is shown in Figure 3.3. The cross sectional figure of the blowdown port is shown in Figure 3.4.

Pressure Vessel Vacuum Computer Simulation

The experimental procedure includes creating a vacuum in the RPV. The purpose of pulling vacuum in the RPV is to evacuate air from the vessel prior to pressurizing it with helium. The data sheet [14] provided no information about the vessel's capabilities to withstand vacuum pressures. A vacuum simulation was performed in Ansys to help

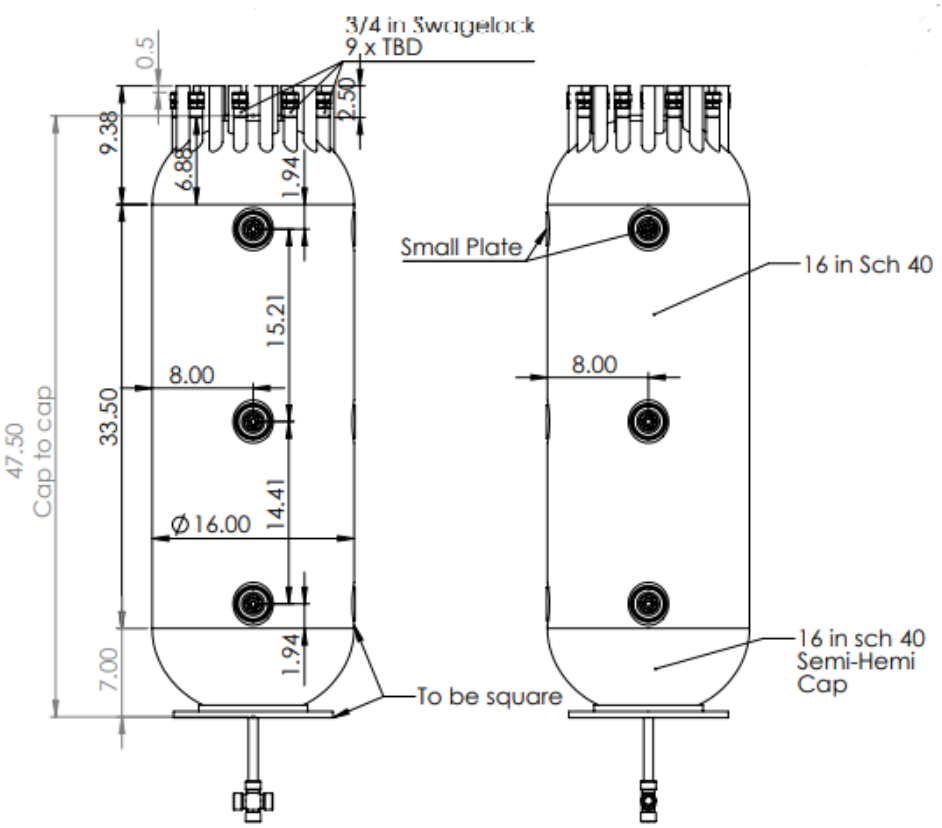

(a) Two sides of the scaled reactor pressure vessel showing where locations where blowdowns can be initiated.

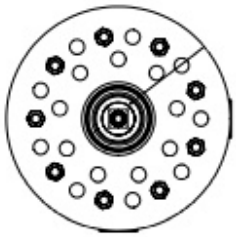

(b) The top of the RPV showing the heating cartridge housings and a large blowdown port.

Figure 3.2: CAD drawings of the top and sides of the reactor pressure vessel where blowdowns can be initiated.

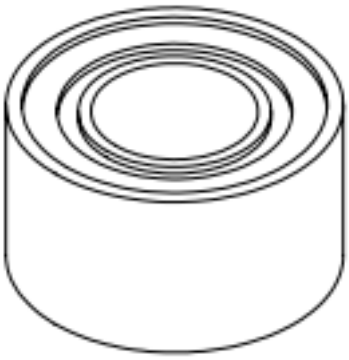

Figure 3.3: CAD drawing of the reactor vessel blowdown port.

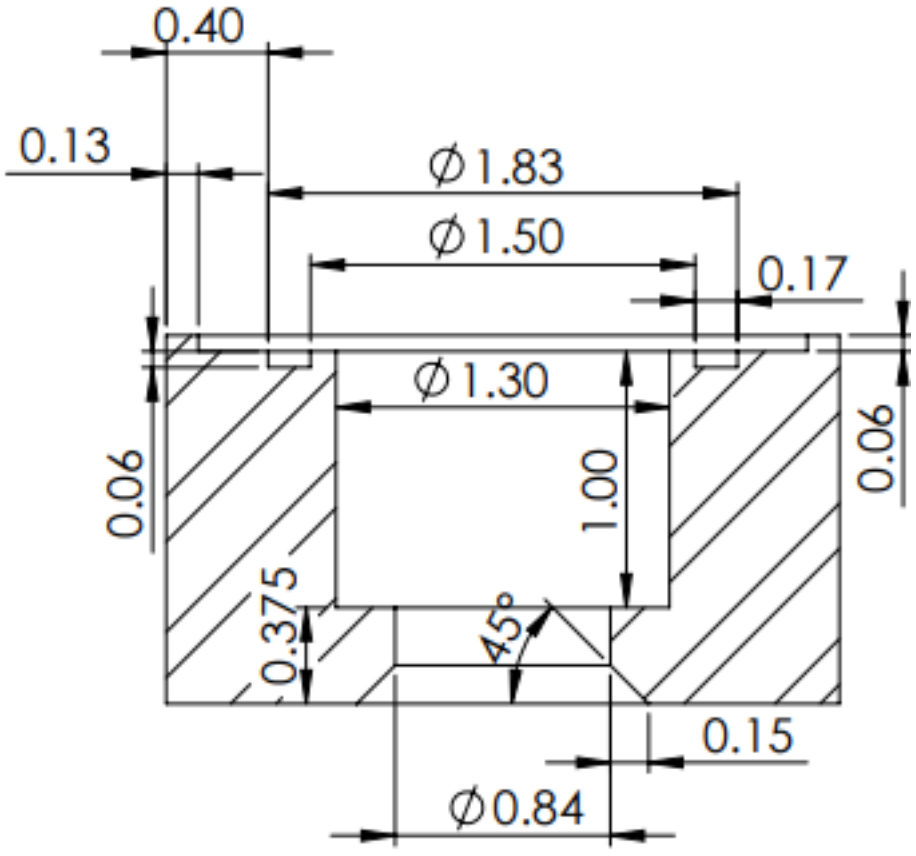

Figure 3.4: The cross sectional cut of the blowdown port.

determine the pressure vessel's ability to withstand sub-atmospheric pressures.

The pressure vessel's original drawings were created using SolidWorks. This file was converted into a Parasolid file and then entered into Ansys. By using Tresca's theory, the required pressures to cause the pressure vessel to structurally fail were determined. The factor of safety for stainless steel 316 was also calculated by using Equation 3.1:

$$\text{FOS} = \frac{\sigma}{2 * \tau} \tag{3.1}$$

where FOS is the factor of safety, σ is the yield strength, and τ is the shear stress. According to ASM Aerospace Specification Metals inc., the yield strength of Stainless steel 316 is 42,100 psi. [15] Applying Formula 1 with a factor of safety of 1 and the given yield strength, the maximum shear stress required for failing is 21,050 psi. This shear stress is obtained by the inside of the pressure vessel being approximately -1975 psi below its ambient pressures. These results suggest that the pressure vessel is capable of withstanding sub-atmospheric internal pressures.

3.1.2 Power Generation Vessel

The PGV, unlike the RPV, is not an ASME stamped pressure vessel. It is not designed to hold pressure and will not be pressurized in the research. This experiment only requires the PGV and a co-axial cross vessel to be present for the modeling exhausted helium flowing through the co-axial cross vessel and containment on its path to an exit port in the PGV containment. Like the RPV, its outer diameter is 16 inches. The height of the cylindrical section is 55.5 inches. The top and bottom caps are respectively 6.88 and 7 inches tall. The total height of the PGV is 69.38 inches.

The PGV fabrication included two steps. First, the middle cylindrical section and the top and bottom caps were purchased from Paramount Supply in Idaho Falls, ID. Second, the three pieces were welded together by WeFab welding in Ammon, ID. The co-axial

cross vessel connects to the PGV 28.55 inches above the bottom of the bottom cap by a hole and a welded nut. The nut has a diameter of $\frac{1}{2}$ inches and 13 threads per inc. Figure 3.5 shows the CAD design for the PGV and its connection to the co-axial cross vessel.

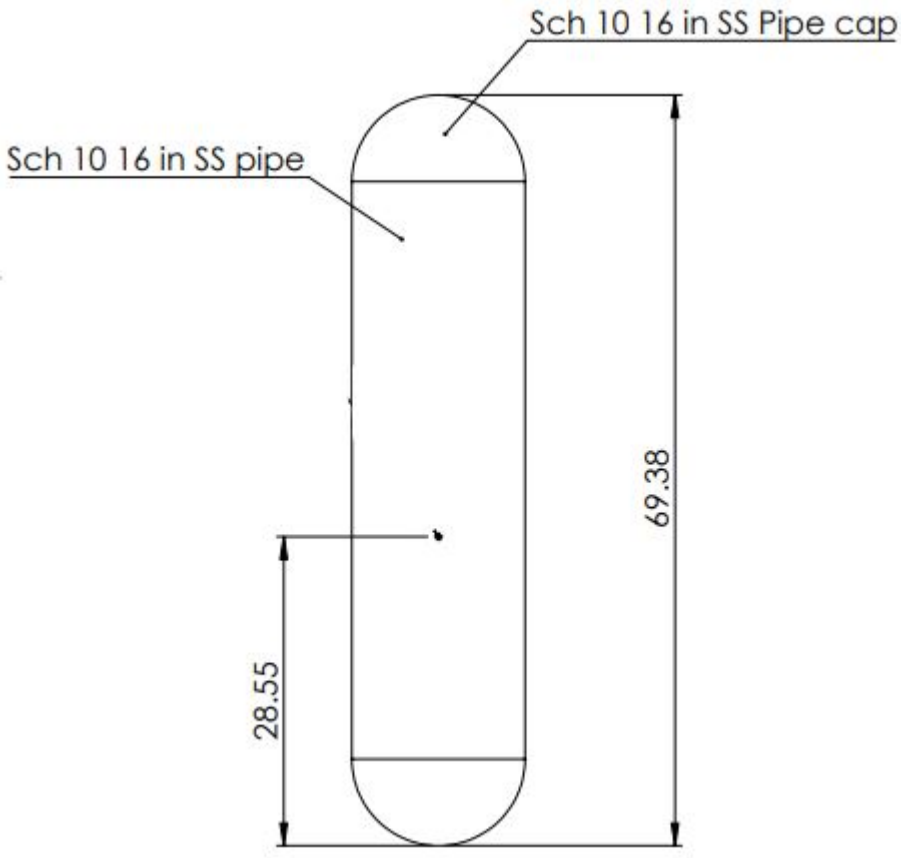

Figure 3.5: The scaled power generation vessel (PGV) showing the drilled-through hole.

3.1.3 Co-Axial Cross Vessel

The co-axial cross vessel is a cylindrical vessel that has ends designed to fit around the curves of both the RPV and the PGV. It is not designed to hold pressure and will not be pressurized in this experiment. The longer ends of the co-axial cross vessel are 11.27 inches long and the shorter sides are 10.63 inches long. A 12 inch 1/2-13 SS bolt goes through the co-axial cross vessel to enter into the PGV. The inside of the co-axial cross vessel contains two walls, 9 inches apart, that the bolt threads through. Figure 3.6 shows

the CAD images depicting the exterior of the co-axial cross vessel and a cross-section cut down the middle.

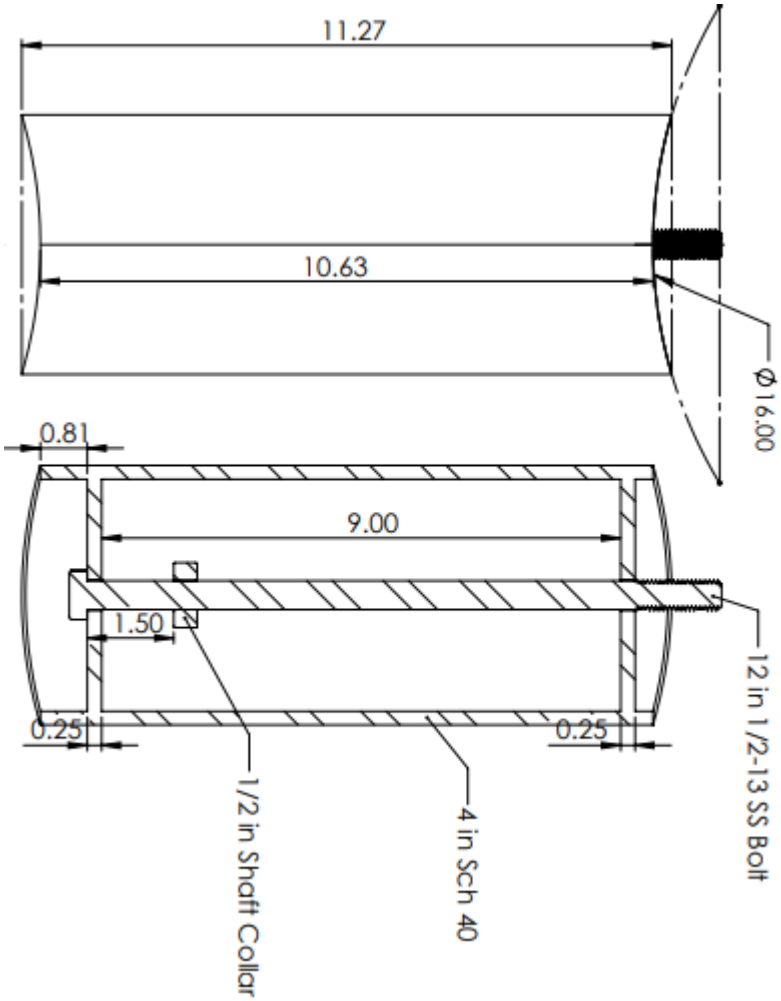

Figure 3.6: The co-axial cross vessel and its cross section, showing the bolt that connects it to the PGV.

3.1.4 Containment Structure

A carbon-steel containment structure surrounds both vessels and the co-axial cross vessel. The volume between the pressure vessel and the containment structure is where most of the helium and air mixing will occur and is the primary location where data will be acquired during experimentation. Windows built into the containment enable blowdowns

to be initiated from different parts of the pressure vessel. The windows are also locations where the containment structure can be vented following the blowdown. The containment composes of five pieces held together by $\frac{5}{16}$ inch screws. These five pieces include the pressure vessel containment structure, scaled power generation dummy vessel containment structure, the upper containment box, the upper containment plate, and the co-axial cross vessel containment. Each component is described in the following subsections. CAD drawings and pictures show the computer design and the construction of each component.

RPV Containment Structure

The RPV containment is a square carbon-steel containment with 20.5 inch side lengths and a height of 32.5 inches. Figure 3.7a shows the CAD drawing of the containment for the RPV. Four windows are built into the RPV containment. The windows in the containment serve as potential locations to initiate a blowdown or vent the containment following a blowdown. Figure 3.7a only shows two windows permitting blowdowns and ventilation. The other two windows are at similar heights, but on different sides of the containment. Figure 3.7b shows the constructed pressure vessel containment with the pressure vessel inside.

PGV Containment

The containment for the PGV is a carbon-steel square containment similar to the RPV containment. The side lengths of the PGV's containment measure 20.5 inches. It is 56.13 inches tall. The window shown on the bottom of the figure is a potential ventilation location. Two windows are built into the PGV containment. They are potential ventilation locations. Only one window is shown in Figure 3.8a. The second window is at the same height, on an adjacent side. Figure 3.8b shows the constructed PGV containment with the vessel inside.

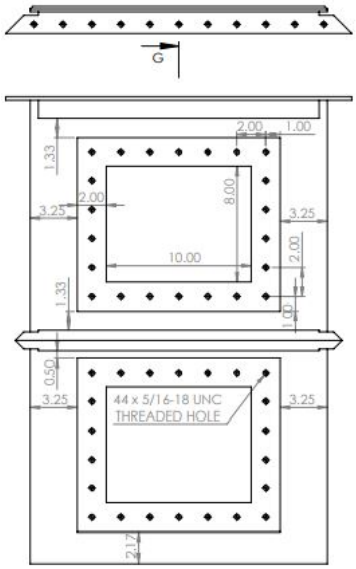

(a) CAD drawing of the carbon-steel RPV containment structure.

(b) The pressure vessel containment structure with the pressure vessel inside.

Figure 3.7: The CAD drawing and real image of the pressure vessel's containment structure.

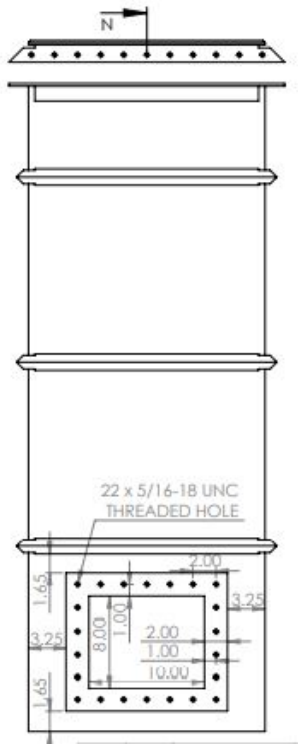

(a) CAD drawing of the carbon-steel PGV containment structure.

(b) The PGV containment structure with the vessel inside.

Figure 3.8: The CAD drawing and real image of the pressure vessel's containment structure.

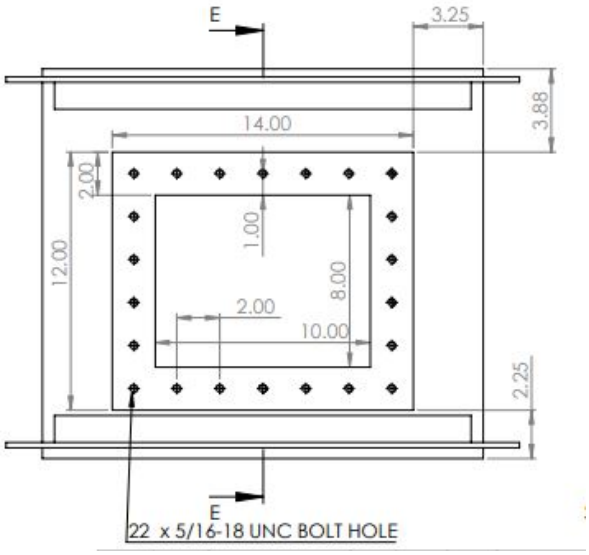

(a) CAD drawing of the upper containment on top of the RPV and PGV containment structures.

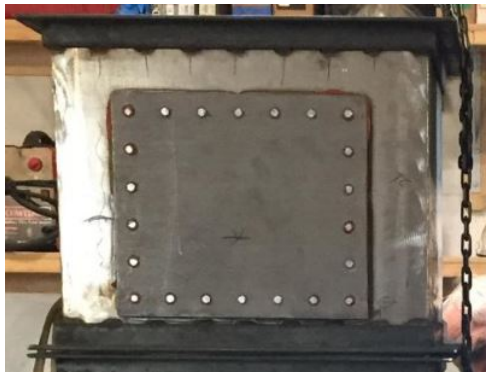

(b) The upper containment on top of the RPV and PGV containment structures.

Figure 3.9: The CAD drawing and real image of the upper containment portion of the RPV and PGV containment structures.

Top Containment Structure

The containment for the RPV and PGV do not cover the entire vessels. A cap goes on top of each vessel's containment. Similar to the other containment sections, the square upper containment has side lengths of 20.5 inches. It is 18.13 inches tall. It has a lip on top permitting a plate to attach to the containment it rests upon. Figure 3.9a shows the CAD drawing of the upper containment. Figure 3.9b shows the back side of the upper containment.

Upper Containment Plate

The square plate covering the upper containment seals the top of the containment. It has 23.88 inch side lengths and attaches to a lip on the upper containment. The lip on the upper containment permits a high temperature gasket to fit between the upper containment plate and the upper containment, creating a gas-tight seal. The plate has a 2.38 inch diameter hole in each corner. These holes enable an oxygen sensor shaft, discussed in section 3.1.5, to be placed at each corner of the RPV containment. The plate is secured to the upper containment by a flange with 44 threaded holes for $\frac{5}{16}$ inch screws. A high temperature gasket is placed between the plate and the upper containment. The plate compressing on the high temperature gasket makes a gas-tight seal with the upper containment. Figure 3.10a shows the CAD drawing the top plate and Figure 3.10b shows the top plate attached to the containment structure. It shows the four locations of thermocouples and the oxygen sensor shaft housing.

Co-axial Cross Vessel Containment

The containment structures surrounding both vessels are connected by the co-axial cross vessel containment. Figure 3.11a shows the axial view of the co-axial cross vessel containment. This figure shows the bolt holes in the co-axial cross vessel containment's flange. These holes line up with threaded holes in the pressure vessels' containment structures. It also has a lip that holds a high temperature gasket. The co-axial cross vessel containment is shown from two angles in Figure 3.14. Figures 3.11a shows the CAD diagrams of the co-axial cross vessel containment structure. Figure 3.11b shows the co-axial cross vessel containment connecting the RPV and PGV containment structures.

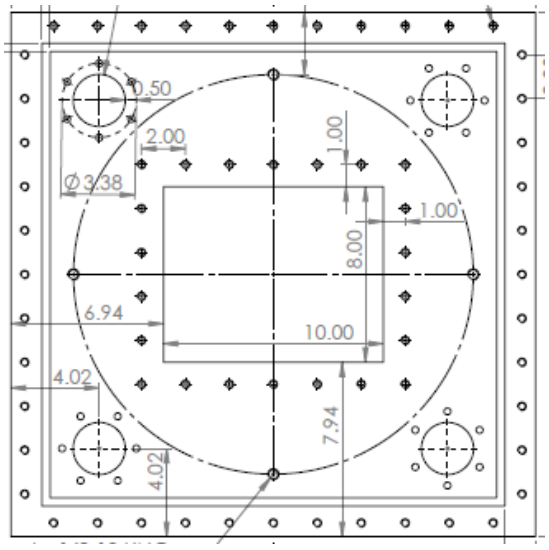

(a) CAD drawing of the top plate.

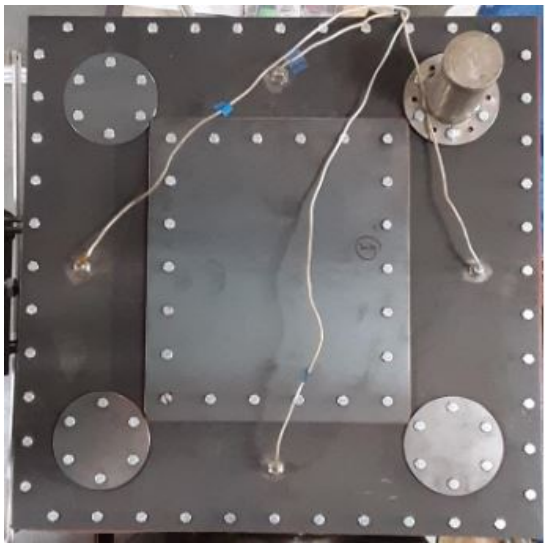

(b) The top plate showing the thermocouples inserted and the oxygen sensor shaft housing.

Figure 3.10: The co-axial cross vessel containment connecting the RPV and PGV containment structures shown axially and from a side view.

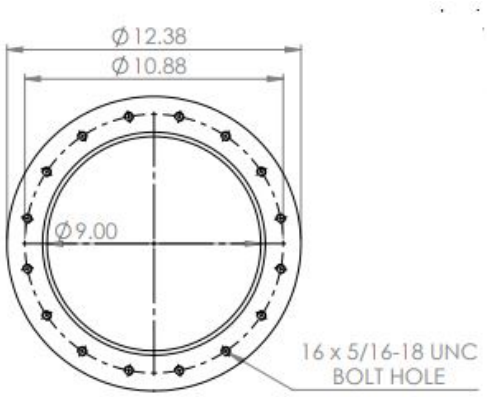

(a) The axial view of the co-axial cross vessel containment.

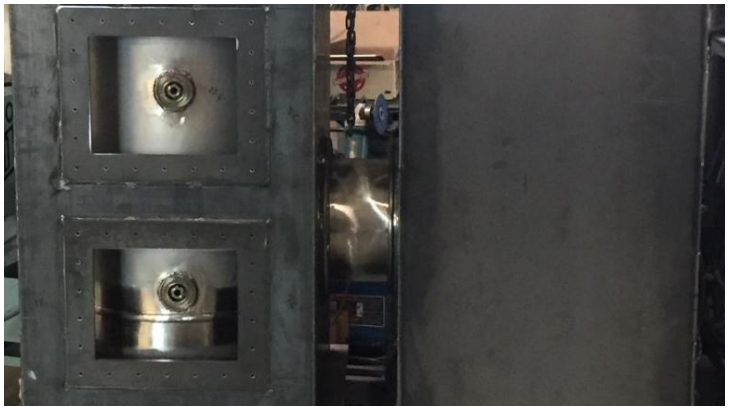

(b) The co-axial cross vessel containment connecting the RPV and PGV containment structures.

Figure 3.11: The co-axial cross vessel containment connecting the RPV and PGV containment structures shown axially and from a side view.

The front view of how the RPV containment, the PGV containment, the upper containment box, and the upper containment lid come together is shown in figure 3.12.

3.1.5 Oxygen Sensor Shaft

The RPV containment houses an oxygen sensor shaft. The oxygen sensor shaft is composed of an all-thread post, an angle iron, an oxygen sensor mounting bracket, and two housing mounts. The housing mounts are attached to the top and bottom of the containment structure and holds the entire oxygen sensor shaft in place. The all-thread post has a diameter of $\frac{3}{16}$ inches with 16 threads per inch. The all-thread post passes vertically

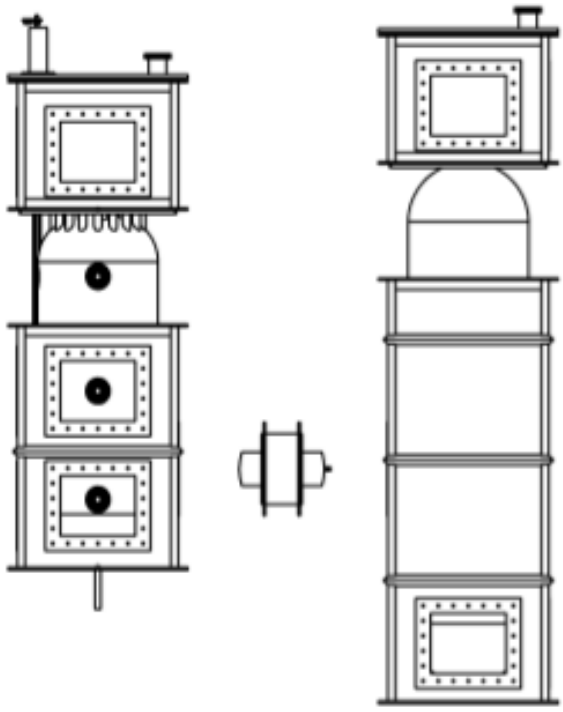

Figure 3.12: An exploded view of how the vessels, their containment structures, and the co-axial cross vessel assemble.

through a threaded hole in the oxygen sensor mounting bracket. The all-thread and angle iron run parallel to each other. They both extend beyond the top and bottom of the RPV containment into the housing mounts. They are anchored by grooves in the housing mounts and by hooks built onto the mounting bracket. As the all-thread spins, the oxygen sensor mounting bracket is prevented from spinning by the angle iron. By rotating the all-thread post, the oxygen sensor attachment bracket can be moved vertically to any position from the top to bottom of the RPV containment. Figures 3.13a and 3.13b show the mounting bracket and the assembly of the mountain bracket, the all thread, and the angle iron.

(a) Oxygen sensor mounting bracket.

(b) The assembly of the oxygen sensor mounting bracket, the all thread, and the angle iron.

Figure 3.13: The co-axial cross vessel containment connecting the RPV and PGV containment structures shown axially and from a side view.

The housing mounts attach to the top and bottom of the RPV containment. Figures 3.14a and 3.14b show the inside and outside of the mounts that house the oxygen sensor shaft. The housing mounts are also visible in Figure 3.12 on top of the containment structure.

(a) The grooves for the all thread and angle iron inside of the oxygen sensor shaft housing.

(b) The outside of the oxygen sensor shaft housing.

Figure 3.14: The co-axial cross vessel containment connecting the RPV and PGV containment structures shown axially and from a side view.

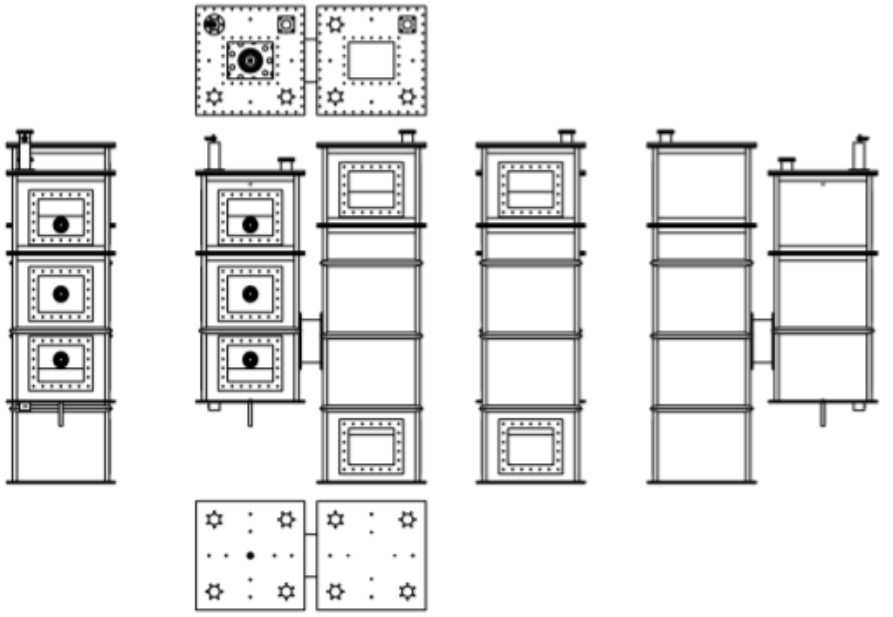

Figure 3.15: All sides of the $\frac{1}{20}$th scaled VHTR. The far left figure depicts the left side of the apparatus. The second figure from the left depicts the front of the apparatus and the top and bottom plates of the containment structure. The second figure from the right depicts the right side of the apparatus. The far right figure depicts the back of the apparatus.

3.1.6 Ventilation

Part of the objective is to determine the amount of oxygen left in the containment after depressurization. To accomplish this goal, a ventilation port was designed to permits gases to escape from the containment structure during the depressurization of the RPV. The ventilation port is also necessary to ensure that pressure does not build up inside the RPV and PGV containment, as the containment structure is not rated or designed to hold pressure.

The ventilation port is a three-part structure. All parts of the ventilation port are built with a carbon steel metal plate. The first part is a mounting flange that attaches the port to the containment structure. The mounting flange that attaches to the containment structure is 14 inches wide and 12 inches high. A rectangular duct attached to the

mounting flange is 10 inches wide and four inches high. The rectangular duct extends four inches from the mounting flange. A second flange opposite to the mounting flange is attached to the rectangular duct. A hinged door is attached to the second flange. This door is opened during the vent the RPV and PGV containment. The ventilation door is closed by $\frac{5}{16}$ inch screws after the blowdown is complete. The ventilation port is shown in Figure 3.16.

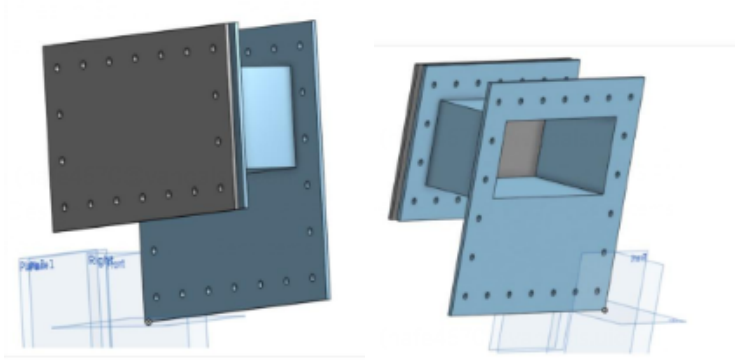

Figure 3.16: CAD figures showing the front flange on the ventilation port (left) and the back flange on the ventilation port (right).

3.1.7 Cooling Tube Manifold

A cooling tube manifold attaches to the bottom of the RPV and extends below the RPV containment. It houses instrumentation used to gauge the pressure and gas concentrations inside the RPV before and during the blowdown. The cooling tube cools the gas to functional temperatures suitable for the attached instrumentation. The instrumentation attached to the cooling tube includes a rigid RTD or thermocouple, an electronic pressure transducer, two manual pressure gauges, an oxygen sensor, and a pressure release valve rated at 400 psig. One manual pressure gauge is rated for pressures between 0-300 psig. The second manual pressure gauge is rated for pressures between -30 inches mercury below atmospheric pressure to 100 psig. Figures 3.17 and 3.18 depict the cooling tube manifold under the RPV. Figure 3.17 shows the manifold's piping and instrumentation

diagram. Figure 3.18 shows the cooling tube manifold attached beneath the RPV.

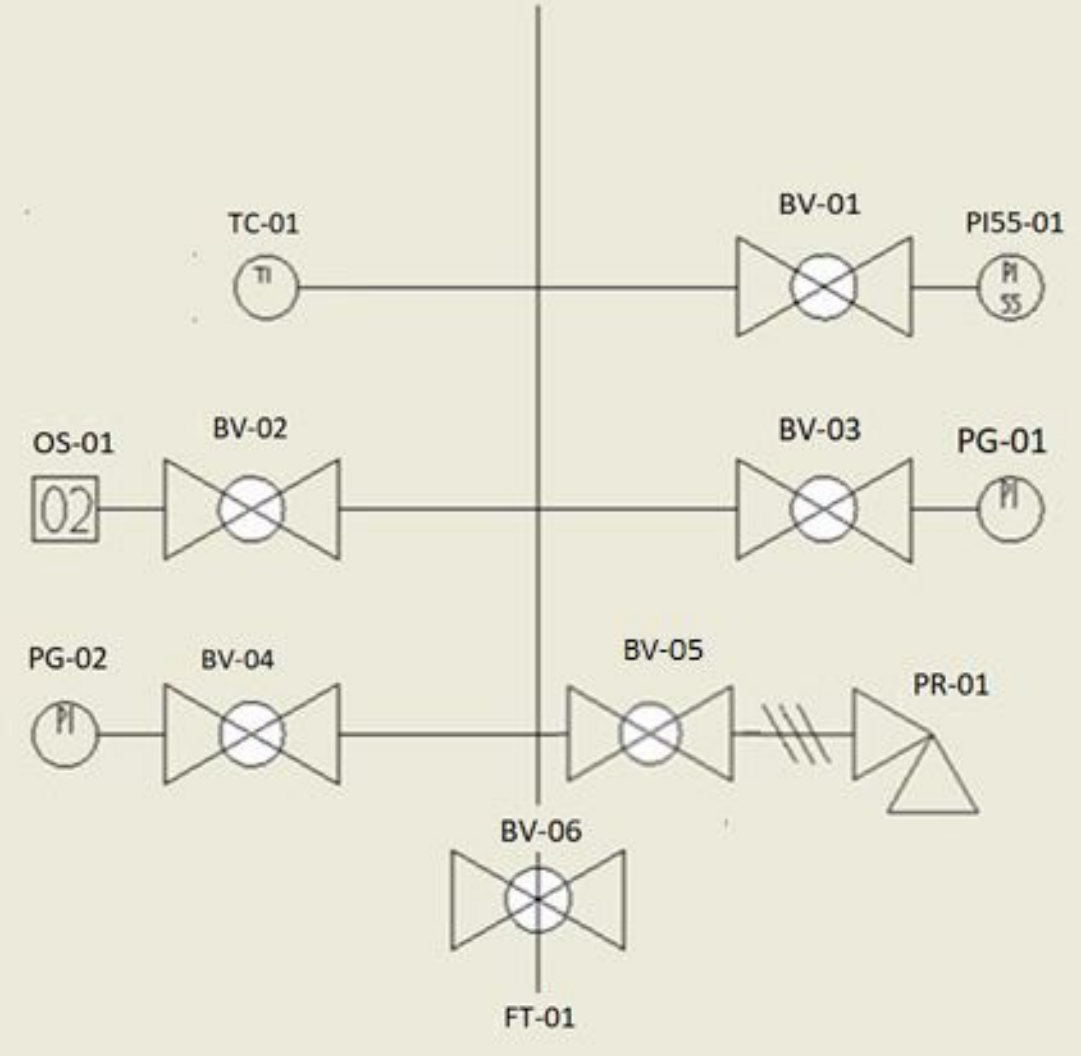

Figure 3.17: Cooling Tube Manifold P&ID Diagram

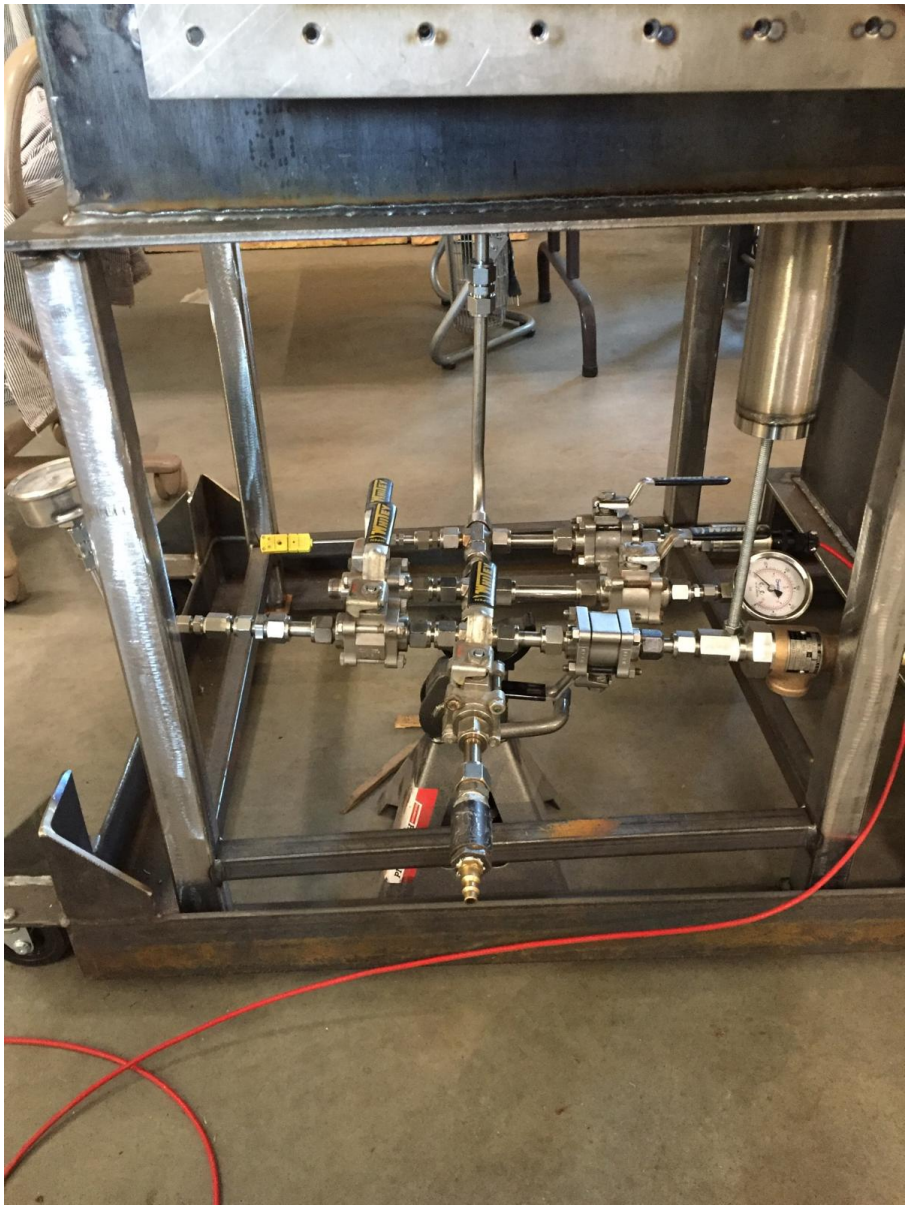

Figure 3.18: Cooling tube manifold with all instrumentation attached including the thermocouple, two manual pressure gauges, one electronic pressure transducer, one pressure release valve, one port for the oxygen sensor, and the fill tube.

3.2 Instrumentation

This section discusses the instrumentation used for the present research and the tests performed to verify the equipment's accuracy prior to experimentation.

3.2.1 Pneumatic Ram

In collaboration with Brigham Young University-Idaho, the University of Idaho designed a pneumatic ram to create a gas-tight seal around the blowdown port of the RPV. This leak-tight seal is formed by a high-temperature gasket between a the blowdown port and a plug. The plug is attached to a rod which extends to an opposing pressure cylinder. The opposing pressure cylinder is supported by a structure which attaches to the containment around the RPV. As the pressure in the opposing pressure cylinder is released, the pneumatic ram retracts and initiates the blowdown. The pneumatic ram that was pressed against the RPV's blowdown port retracts and presses against a gasket on the inside of the containment structure. It prevents gases from exiting the containment through the pneumatic ram's access port.The pneumatic ram is shown in Figure 3.19.

Figure 3.19: Testing the pneumatic ram.

The pneumatic ram's ability to hold pressure was tested prior to experimentation. It effectively held 300 psig during a hydrostatic pressure test.

3.2.2 Heating Cartridges

The helium in the RPV is heated by 5 custom designed heating cartridges manufactured by Maxiwatt Inc. The heating cartridges are mounted to the $\frac{3}{4}$ inch threaded holes in the top of the RPV by swagelok fittings. The heating cartridges are 43.5 inches long with a 10-inch dead zone at the top. They produce 1500 watts at 240 volts. The cartridges have four 90 inch lead wires and two thermocouple wires extending from the top. The two thermocouple wires form a K-type thermocouple at the end of the heating cartridge. The other four wires provide power to the two heating elements within the heating cartridge. All six wires are fiberglass insulated and can withstand temperatures up to 750° C. Figure 3.20 shows the heating cartridge's wiring schematic. It also shows the thermocouple joint shown on the left of the image.

The heating cartridge wires exit locations are shown in Figure 3.21. The top row of swagelok fittings welded to back of the top containment are for 10 lead wires to exit the containment structure, even though there are 20 lead wires between the five cartridges. Ten lead wires were cut and soldered together to be wired into a parallel circuit.For this reason, only 10 of the 20 lead wires exit the containment structure. Below the lead wires inserts are two rows of 5 swagelok fittings. These two rows of swagelok fittings allow the heating cartridge's thermocouples to exit the containment.

Two swagelok fittings are welded to the bottom of the containment. They allow thermocouples to enter the containment for data acquisition. They are discussed later in section 5.2.

Preliminary Heat Tests

Heating tests were performed inside the RPV prior to experimentation. Four heating cartridges, wired in parallel, were supplied power by Model TPC-1000 Tempco power

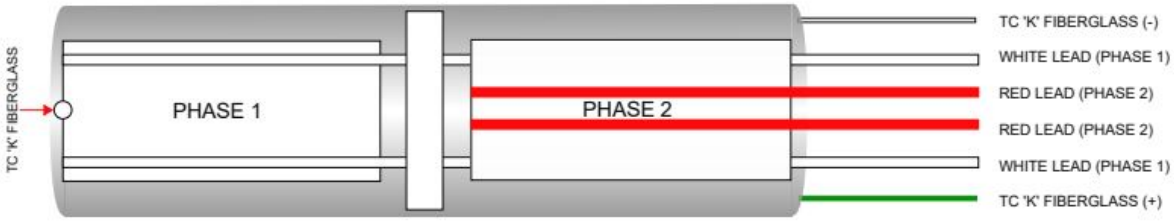

Figure 3.20: The wiring schematic and thermocouple joint in the Maxiwatt heating cartridge. The elements labeled Phase 1 and Phase 2 represent both heating elements inside of the cartridge and their lead wires.

Figure 3.21: Thermocouple and heating cartridge wire locations on the back side of the top of the RPV containment structure.

controller. The power controllers were programmed to raise the temperature of the cartridges to 250° C at a rate of 10° C per minute. The initial pressure and temperature of the RPV was 19° C. Its initial pressure was 130 psig. The increase of temperature and pressure during the heat test are shown in Table 3.1.

Table 3.1: Temperature and pressure values during a preliminary heating test in the RPV.

Time (min)	Temperature (°C)	Pressure (psig)
10	87	156
20	201	199
30	234	212
40	257	224
50	268	229
60	274	233

Vertical heating tests were performed with the cartridges in an open environment a room temperature. The heating cartridges were powered by 120V power supplies. After the cartridge reached thermal equilibrium, the bottom and tops of the cartridge were respectively 199° C and 224 ° C. The temperature gradient between the top and bottom of the cartridges was 25° C. Similar to the vertical heating test at room temperature outside of the pressure vessel, a temperature gradient was found inside of the pressure vessel during preliminary heating tests. Table 3.1 reports data on a heating test performed inside of the RPV. The thermocouples at the bottom of the cartridges read at 250° C. A rigid thermocouple inserted into a middle blowdown port read 274° C. That indicates a 24° C temperature gradient between the bottom and middle of the RPV.

The pressure in the RPV during the heating test does not reach 250 psig, which is the desired experimental pressure. This is because the pressure inside the RPV was not high enough prior to heating the system. In order for the RPV pressure to reach 250 psig when it is heated to 250° C, the pressure must be 140 psig before the system is heated.

3.2.3 Oxygen Sensors

The oxygen sensor data acquired in the RPV containment is essential to understand the mixing patterns of helium and air following a blowdown. The oxygen sensor measures the percentage of oxygen in the space between the outer wall of the RPV and the inner wall of the RPV containment. As hot helium is released from the RPV, the oxygen sensor measures the decrease in oxygen as it is displaced by helium.

The oxygen sensors for this experiment were required to meet multiple key specifications. First, the sensors needed to be small enough to fit in the void space between the RPV and the RPV containment. Second, the sensor and connecting instrumentation wires need to withstand 250° C.

The oxygen sensors that best met those requirements are Honeywell's GMS-10-RVS oxygen sensor. This oxygen sensor has a diameter of 12 millimeters (0.47 inches) and is 83 millimeters long (3.27 inches). [16]

The oxygen sensor's wires were tested to withstand the experimental pressures temperatures by putting a section of the wire into an oven. Table 3.2 shows an experiment performed to ensure that the oxygen sensor's wires could endure the experimental temperatures.

Table 3.2: Values used to calculate thermal hydraulic properties of the prototype

Temp (deg F/C)	Time/Transition Time	Time at Temp	Wire Condition
170/76.666	12:50 PM (start)	60 min	Solid
215/101.667	1:50 PM/2 min	50 min	Solid
250/121.111	2:40 PM/2 min	30 min	Solid
400/204.444	3:40 PM/4 min	60 min	Solid
450/232.222	4:30 PM/1.5 min	50 min	Solid

Figure 3.22: Air-tight containment.

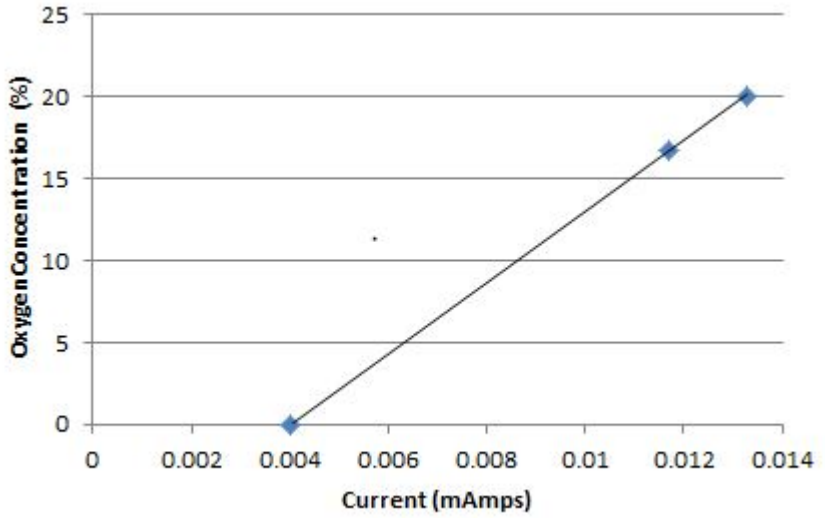

Figure 3.23: Data acquired to calibrate the oxygen sensor.

Oxygen Sensor Calibration

The oxygen sensors were calibrated in an air-tight system. The system was built by connecting four $\frac{1}{2}$-inch stainless steel tubes to a Swagelok cross. These four stainless steel tubes were attached to a manual pressure gauge, a gas fill tube, a vacuum tube, and the oxygen sensor. The pressure gauge, gas fill tube, vacuum tube, and oxygen sensor tube are all isolated by valves. To calibrate the oxygen sensor, the air was purged from the system by a process of vacuuming and filling. The gas used to calibrate the oxygen sensor was an 80/20 concentration of nitrogen and oxygen. After purging the system and filling it with the 80/20 concentration of nitrogen and oxygen, data points were taken to calibrate the oxygen sensor. The air-tight containment used to calibrate the oxygen sensor is shown in Figure 3.22. Figure 3.23 shows the data points acquired to calibrate the oxygen sensors.

The data shown in Figure 3.23 shows that the oxygen sensor data is linear. The oxygen sensor's readings of air at room temperature and the 80/20 concentration of nitrogen and oxygen were nearly identical. After the oxygen sensor was wired with appropriate

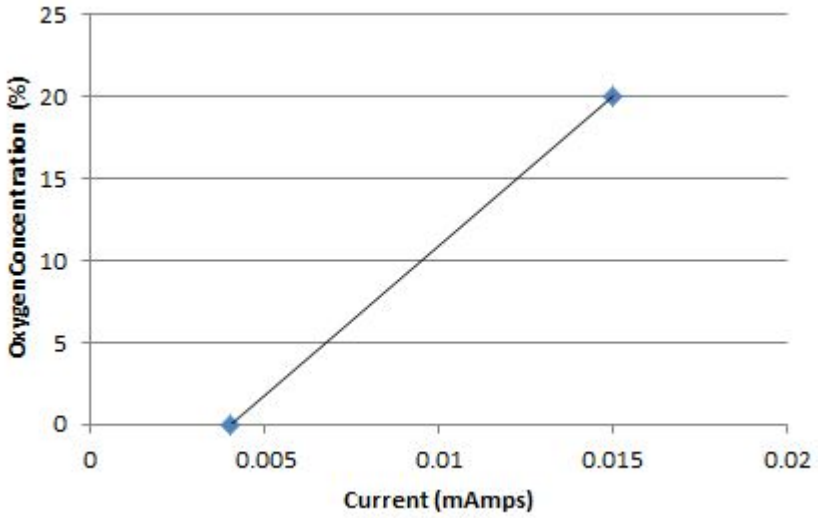

Figure 3.24: Data acquired to calibrate the oxygen sensor.

length wires for experimentation, the oxygen sensor current readings increased from 13.6 milliamps to 15.0 milliamps. Because it was previously determined that atmospheric oxygen concentrations were nearly 20% oxygen, the oxygen sensor could be calibrated again with air at standard atmospheric conditions. Figure 3.24 shows the line used to generate the equation that converts oxygen sensor readings to oxygen concentrations. Equation 3.2 is the equation generated by the line in Figure 3.24, where x represents the milliamp readings from the oxygen sensor.

$$y = 1818.2x - 7.2727 \tag{3.2}$$

Because there are only two points in Figure 3.24, the R^2 value for Equation 3.2 is 1. The GMS-10-RVS oxygen sensor's accuracy is dependent on pressure. It is rated to be accurate within five mbar. [16] The accuracy of the pressure transducer is five mbar divided by the pressure of the gas being evaluated. If an experiment is performed at atmospheric pressure, which is approximately 1013 mbar, the accuracy of the oxygen sensor is within 0.49% above or below the actual oxygen concentration determined by the

oxygen sensor.

3.2.4 Thermocouples

A key part of the data collection process was measuring temperatures in the space between the RPV and its containment. Two-hundred feet of fiberglass insulated type-K thermocouple wire was purchased from Idaho Laboratories, in Idaho Falls, ID. The thermocouples enter the containment through $\frac{1}{8}$ inch holes. An air tight seal is created around the thermocouple wire with a Swagelok fitting and teflon ferrules. A pressure test was performed to ensure that an air-tight seal formed between swagelok fittings, teflon ferrules, and the fiberglass insulation. This was done by inserting a thermocouple wire into an air-tight tube, closed down on by teflon ferrules and a swagelok fitting. A pressure gauge was attached to opposite end of the tube. The tube was pressurized to 5 psig and then was placed under water. The swagelok fittings and teflon ferrules proved to be effective as no bubbles were observed and the tube maintained pressure at 5 psig.

Thermocouple Calibration

Thermocouples were calibrated by comparing their measurements to a calibrated four-wire resistance temperature device (RTD). The four-wire RTD was purchased from Idaho Laboratories in Idaho Falls, ID. The thermocouples and RTD values were compared while being submerged in ice water and boiling water. The ice water and boiling water gave data points at 0° C and 94.7° C. Oil was used to calibrated the thermocouples at temperatures above 94.7° C. The oil was heated to 180° C, and 220° C. Figure 3.25 shows the thermocouple values plotted against RTD values from Table 3.25. Error bars are included, but the error values are not big enough to be visible. Figure 3.3 shows temperature and error values during the calibration process. The 'RTD Value' column shows the RTD temperature reading. The 'Average TC Value' column shows the average

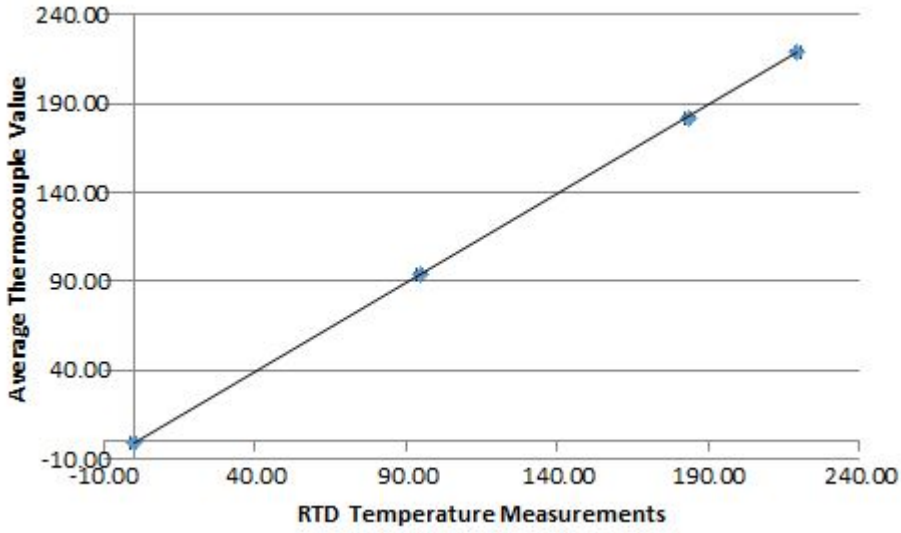

Figure 3.25: Average thermocouple values plotted against RTD values in ice water, boiling water, oil at 180° C, and oil at 220° C. The RTD values and thermocouple values are the numbers shown in the first two columns in Figure 3.25.

Table 3.3: Temperature, error, and standard deviation values shown to calibrate the thermocouples against a calibrated four-wire RTD.

	RTD Value	Average TC Value	TC Standard Deviation	Mean Error
Ice Water	-0.12	-0.62	0.16	0.50
Boiling Water	94.73	94.10	0.74	0.63
180 ° C	183.29	181.76	0.86	1.53
220° C	219.62	219.17	0.51	0.56

of the 23 thermocouples readings. The 'TC Standard Deviation' column shows the standard deviation of the 23 thermocouple readings. The 'Mean Error' column shows the average difference between the thermocouple temperature readings and the RTD temperature readings.

3.2.5 Hot Wire Anemometer

Five FMA-900 series hot wire anemometers were purchased to determine air velocities mixing and exiting the containment structure. Four hot wire anemometers were rated to measure gases moving between 0-10.16 mps. These hot wire anemometers measure the

air velocity exiting the ventilation port. One hot wire anemometer is rated to read air velocity between 0-60.9 mps. It measures the air velocity inside of the containment. The data sheet indicated that their readings are accurate within two percent. [17] The hot wire anemometers are mounted to the containment and ventilation port through $\frac{1}{8}$ inch diameter holes. Swagelok fittings with metal ferrules create a gas-tight fitting around the rigid hot wire anemometers.

Hot Wire Anemometer Calibration

To calibrate the hot wire anemometers, a constant flow of air was generated by connecting an air compressor to a cap on a $1\frac{1}{2}$ diameter pvc pipe. The air velocity could be changed by changing the pressure inside of the air compressor. The diameter of the pvc pipe restricted from $1\frac{1}{2}$ inches to 1 inch. The hot wire anemometers inserted into the pvc pipe near the exit. They were calibrated by comparing their current readings to velocities measured by a Kestrel 5700 Elite. The Kestrel 5700 Elite is rated to read velocities moving 40 $\frac{m}{s}$ with 3% error. [18] Figure 3.26 shows the data acquired to calibrate the hot wire anemometers inside the containment structure. These data points generated Equation 3.3, where x represents the current values from the hot wire anemometers. Figure 3.27 shows the data acquired to calibrate the hot wire anemometers inside the containment structure. These data points generated Equation 3.4, where x represents the current values produced by the hot wire anemometers. The R^2 value for Equation 3.3 is 0.9978 and the R^2 value for Equation 3.4 is 0.9883. The hot wire anemometer data sheet states that they are accurate to within two percent. [17]

$$y = 4052x - 16.248 \tag{3.3}$$

$$y = 918.6x - 3.0262 \tag{3.4}$$

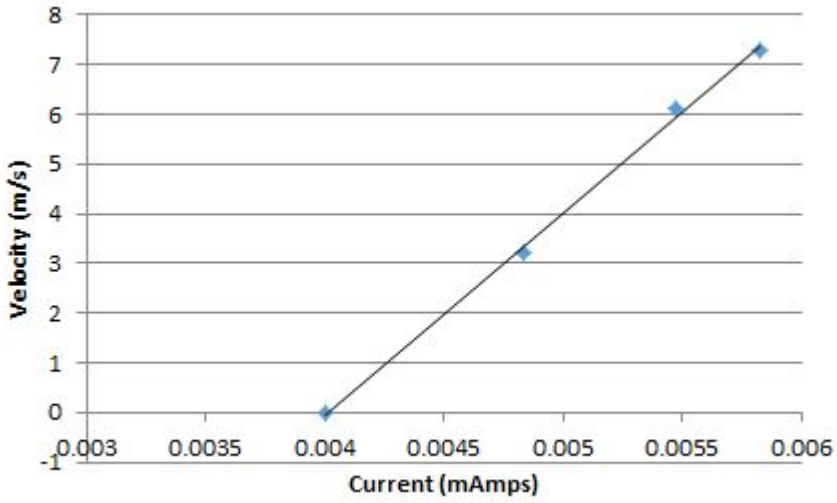

Figure 3.26: Data points to calibrate the hot wire anemometers inside the containment structure.

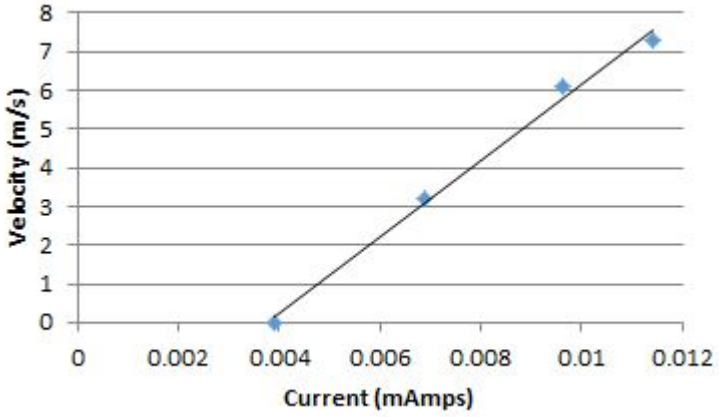

Figure 3.27: Data points to calibrate the hot wire anemometers at the ventilation port.

3.2.6 Pressure Transducer

The PX32B1-100GV pressure transducer was purchased from Omega Engineering to determine the pressure of the RPV during the pressurization process and the blowdown. The PX32B1-100GV pressure transducer is rated to read pressures from 0-300 psig and has a maximum temperature limit of 168° C. The associated mating connector for the PX32B1-100GV attaches to the PT06F10-6S cord for data acquisition. The output is 3 mV/V. [19] The pressure transducer required the DRC-4720 to translate the signal from mV to a range of 4-20 mA. The PX32B1-100GV pressure transducer connects to the cooling manifold. It is labeled in Figure 3.17 as PR-01.

Pressure Transducer Calibration

The equation to convert current readings in milliamps to pressure readings in psig was generated by comparing the electronic data to two manual Swagelok pressure gauges. They are rated to be accurate to within 1.5%. [20] One Swagelok gauge was rated for pressures between 0-100 psig. The second gauge was rated for pressures between 0-300 psig. The RPV was pressurized to 140 psig, and then heated to different temperatures to increase the pressure.The pressures achieved inside the RPV due to heating were 200 psig, and 245 psig. This gave 4 data points to calibrate the pressure gauge against: 0 psig, 140 psig, 200 psig, and 245 psig. The graph of these pressures and the correlating data points are shown in Figure 3.28. The equation generated by these data points is shown in Equation 3.5, where x represents the milliamp readings from the pressure transducer. The R^2 value for the data points is 0.999. The pressure transducer's spec sheet states that it is accurate within 0.25%. [19]

$$y = 17056x - 68.239 \tag{3.5}$$

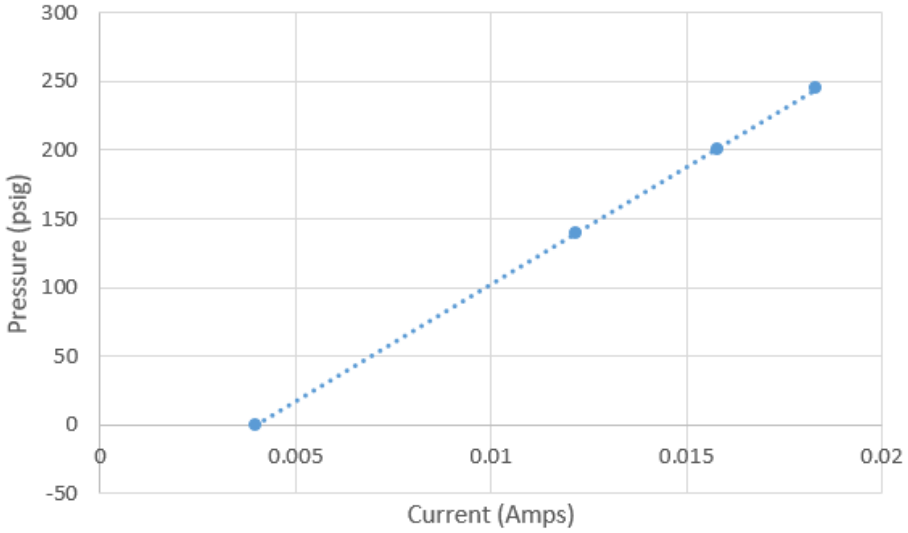

Figure 3.28: Data points taken by the pressure transducer at 0 psig, 140 psig, 200 psig, and 245 psig.

3.3 Experimental Procedures

Before beginning experimentation, the amount of helium required for a single blowdown was calculated with Equation 3.6:

$$V_{He} = \frac{V_{RPV} * C * P_{pre-heat}}{P_{atm}} \tag{3.6}$$

where V_{He} is equal to the volume of helium in cubic feet required to pressurize the vessel to the pre-heated pressure, V_{RPV} is the volume of the RPV in cubic meters, C is the constant that converts cubic meters into cubic feet, $P_{pre-heat}$ is the pressure of the vessel before heating the cartridges, and P_{atm} is atmospheric pressure of air. Given that V_{RPV} equals 0.139 m^3, C equals 35.315 $\frac{ft^3}{m^3}$, $P_{pre-heat}$ equals 140.084, and P_{atm} equals 14.7, V_{He} equals 46.876 cubic feet of helium at standard pressures and temperatures.

To understand the phenomena related to a blowdown of the RPV, eight different blowdown scenarios were determined. Because of facility limitations related to Covid-19 and university requests,the scope of this thesis is limited to reports on preliminary

blowdowns and initial tests. The proposed tests shown in Figure 3.4 will be performed once the apparatus is located at CAES.

Each of the eight blowdowns vary by the location of the blowdown, the location of the ventilation, and the diameter of the blowdown hole. The blowdown locations and locations of instrumentation can be found in Table 3.4. These combinations were decided upon to ensure that each blowdown height had multiple ventilation heights and different hole sizes. The blowdown and ventilation locations are described the being on the front or the side of the containment. The front of the RPV and PGV containment structures are shown in Figure 3.1. When looking at the front of the apparatus, three windows are visible on the RPV containment and two windows are visible on the PGV containment. The co-axial cross vessel containment is also seen connecting both containment structures. The left side of the containment is the adjacent side of the RPV containment structure on the opposite side of the PGV containment structure. By looking at the apparatus from this view, only three windows are shown in the RPV containment. The CAD diagram showing the left side of the apparatus is far left image shown in figure 3.15.

The heights of the blowdown and ventilation locations are described as the bottom, middle, or top locations. Three windows are built into the RPV containment structure. The lowest two windows are referred to as the bottom windows. The highest two windows are referred to as the top windows. The middle windows are referred to as the middle windows. Figure 3.1 shows the blowdown and ventilation locations for blowdowns discussed in Chapter 4. pneumatic ram is in the Top-Front location. The ventilation is located at the Bottom-Front location. The blowdown and ventilation locations for the blowdowns discussed in Chapter 5.

Table 3.4: Blowdown and ventilation locations with the hole size for 8 blowdown tests.

Blowdown Location	Vent Location	Hole Size
Bottom-Left	Top-Left	1/2 inch
Top-Front	Bottom-Front	1/4 inch
Top-Left	Bottom-Front	1/2 inch
Middle-Left	Top-Front	1/4 inch
Bottom-Left	Middle-Front	1/2 inch
Top-Front	Middle-Left	1/4 inch
Middle-Front	Lower-Left	1/2 inch
Lower-Front	Upper-Left	1/4 inch

CHAPTER 4

Predictive Modelling

4.1 Introduction

This section discusses predictive modelling performed on the apparatus. A CFD model was built in StarCCM+ to model the heat transfer and gas mixing patterns following the blowdown. The CFD design matches the geometry of the apparatus including its dimensions, shape, blowdown location, and ventilation location. The second method is an analytical method performed in Python to predict the blowdown time, RPV pressure values, mass flow rates, and exit velocities.

4.2 CFD

Preliminary CFD analysis was performed with StarCCM+ by Silvino Balderrama from the University of Idaho. Because this thesis focuses on testing and validating a scaled VHTR testing apparatus and not providing final results, CFD results were not generated to match the results from the experiments discussed later in this thesis. The insights gained from this CFD analysis aid in constructing and designing the apparatus. The helium/air mixing patterns it describes will aid in instrument placement and identifying specific areas of interest. Several observations from preliminary CFD analysis gave insight to the project design and future works. First, the images in Figure 4.3 suggest that the gas above the co-axial cross vessel is mostly helium and the gas below the co-axial cross vessel is mostly air. This information suggests that during future blowown tests, the oxygen concentration values near the co-axial cross vessel should be more closely evaluated than other areas. Second, CFD streamline predictions also provided insight as to where the fastest gas movements would be inside the containment structure during the blowdown. This information led to placing a hot wire anemometer inside of the

Table 4.1: Simulation parameters for the CFD model.

Simulation Parameter	Value
Turbulence Model	$k - \omega$
Time Step	10^{-5} seconds
Total Time	5.5 seconds

containment structure.to measure gas velocities. Finally, the ventilation port dimensions and gas flow patterns were carefully considered in the preliminary calculations. Streamline predictions and the stratification demonstrated in the ventilation port shown in Figure 4.3b further demonstrate that the gas patterns in the ventilation port are indicative of the overall flow. For this reason, careful consideration was taken when placing hot wire anemometers and thermocouples in the ventilation port.

Two images in Figure 4.1 show the geometry built in StarCCM+. This geometry matches the blowdown port and ventilation port locations of the blowdowns discussed later in this thesis. It is the same configuration shown in Figure 3.1. The blowdown is initiated at the top blowdown port on the front side of the apparatus. The ventilation port is also on the front side of the apparatus at the bottom window. Figure 4.1a shows the exterior of the geometry. Figure 4.1b shows a slice of the containment, showing the internal configuration of the containment structure, the RPV, and the gases inside each volume. Figure 4.2 shows the geometry's mesh. This analysis was performed with helium. The simulation's parameters are shown in Table 4.1.

The simulation's prediction of air and helium mixing patterns at 5.5 seconds are shown in the images shown in Figure 4.3. Figure 4.3a shows the mass fraction predictions. It suggests that the majority of the gas inside the RPV containment structure above the co-axial cross vessel is helium. It also suggests that the majority of the gas inside the containment structure below the co-axial cross vessel is air. Figure 4.3b shows similar results by showing the molecular weight. The gas inside the top of the co-axial cross vessel is primarily helium. The gas at the bottom of the cross vessel is mostly air. The

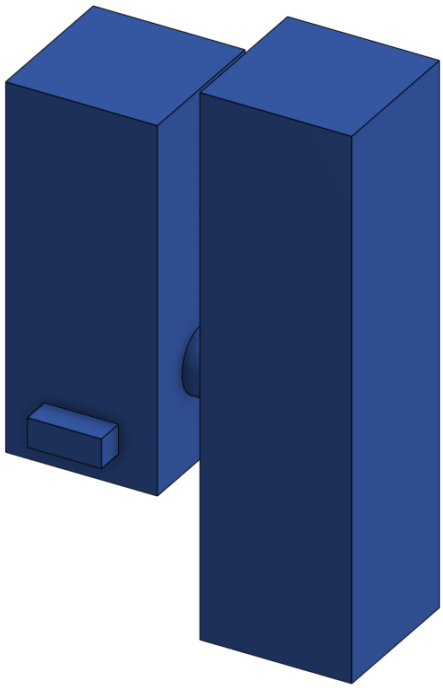

(a) The CFD structure designed in StarCCM+ matching the blowdown port and ventilation port locations.

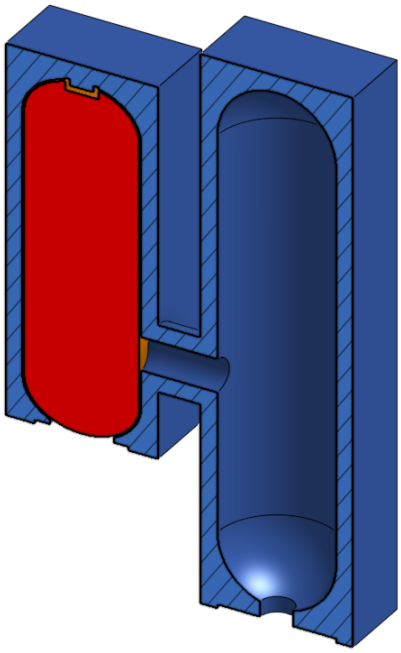

(b) The slice of the CFD design used to show the gas flow patterns inside the containment structure.

Figure 4.1: The geometry of the structure built into StarCCM+ to perform CFD analysis on the $\frac{1}{20}$th scaled VHTR model.

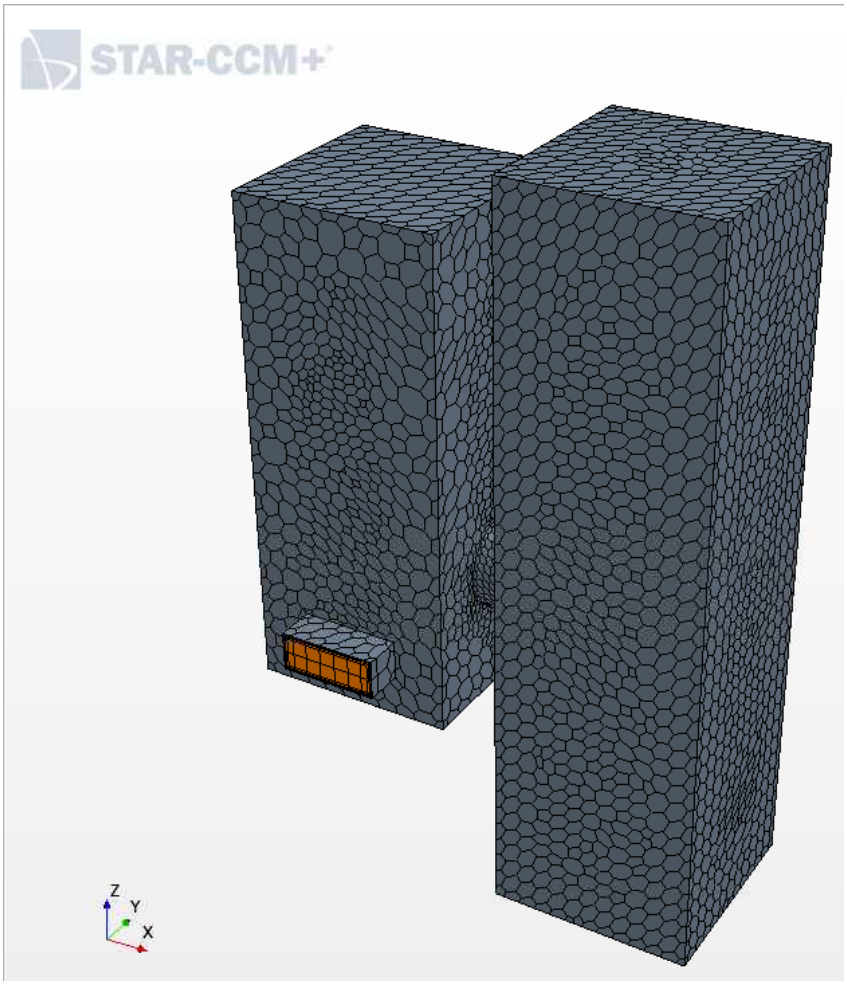

Figure 4.2: Mesh of the CFD geometry designed in StarCCM+.

co-axial cross vessel seems to be the location where the helium concentrations decrease and air concentrations increase in the RPV containment structure. This is because the helium enters into the PGV containment structure through the top of the co-axial cross vessel. As the helium enters the PGV containment structure, air in the PGV containment structure exits through the bottom of the co-axial cross vessel into the RPV containment structure.

4.3 Analytical Solutions

Python was used to analytically predict the blowdown time, pressure, mass flow rate, and exit velocity values during the blowdown time. These calculations use the methodology of Arcilesi [11], but are applied to the apparatus constructed as part of this thesis. Table 4.2 states the system's initial conditions used to determine the pressure, exiting mass flow rate, and exit velocities from the RPV.

Table 4.2: Initial conditions of the blowdown apparatus prior to performing the blowdown.

Variable	Value	Units
Internal Pressure	250	psig
Internal Temperature	250	Celsius
Exit Pressure	0	psig
Exit Temperature	27	Celsius
Internal Gas Density	1.68	$\frac{kg}{m^3}$
External Gas Pressure	1.225	$\frac{kg}{m^3}$
Internal Gas Viscosity	3.925* 10^-5	Pa*s
External Gas Viscosity	1.87 * 10^-5	Pa*s

The primary driving force for the exit velocity is the difference in pressure between the RPV and its containment structure. The equation to determine the velocity is found in Equation 4.1:

$$v_{guess} = \sqrt{\frac{(P - P_{amb})}{\rho_{avg} * (\frac{\alpha}{2} + 0.5 * (k_c + f_{guess} * \frac{L}{D})}} \tag{4.1}$$

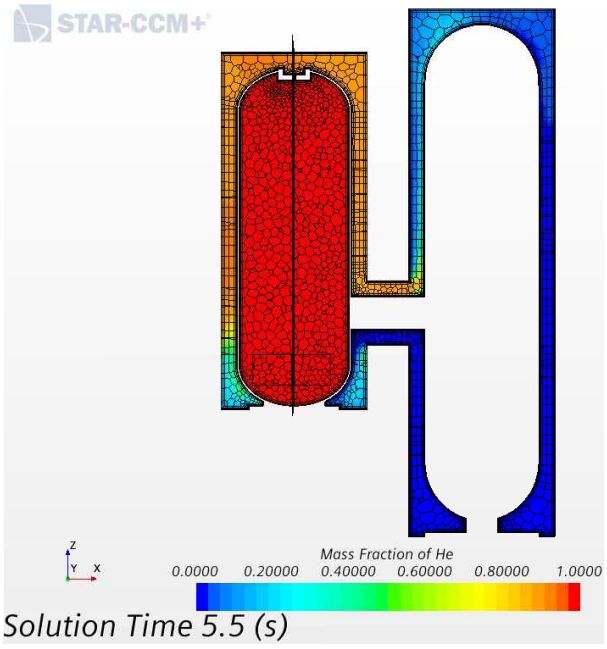

(a) CFD mass fraction prediction.

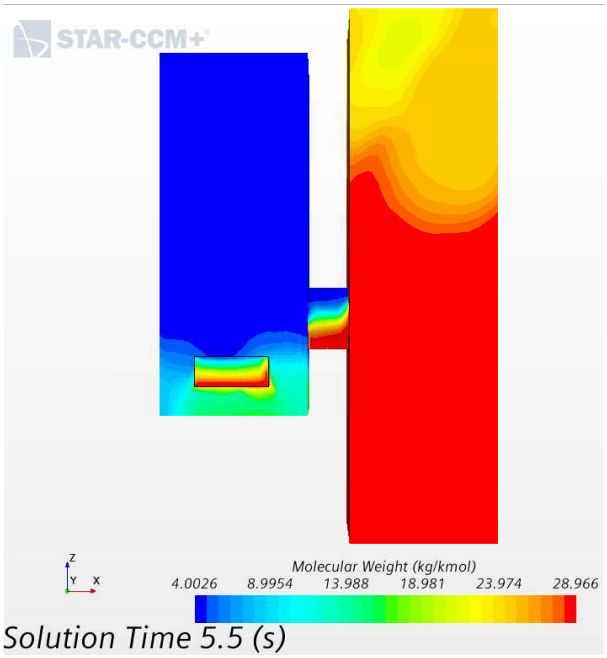

(b) CFD molecular weight prediction.

Figure 4.3: Mass fraction and molecular weight predictions at 5.5 seconds in the StarCCM+ CFD model of the $\frac{1}{20}$th scaled VHTR model.

where P is the pressure inside of the RPV, P_{amb} is the ambient pressure, ρ_{avg} is the average density of the gases inside and outside the RPV, α is the kinetic energy coefficient, k_c is the loss coefficient for sudden contraction, f_{guess} is the friction factor. L is the length of the exit orifice, and D is the diameter of the exit orifice.

Equation 4.1 provides only a guess of the velocity, instead of calculating the expected velocity. This is because of its dependence on a guess for the friction factor, f_{guess}. To determine the velocity of the gas exiting the experimental RPV, the friction factor is first determined by an iteration process shown in Equation 4.2:

$$\begin{aligned} f(i+1) &= \left(\frac{1}{\left(\frac{-2*\ln\frac{eps}{D}}{3.7}\right)+\left(\frac{2.51}{Re*\sqrt{f(i)}}\right)}\right)^2 \\ f(i+2) &= \left(\frac{1}{\left(\frac{-2*\ln\frac{eps}{D}}{3.7}\right)+\left(\frac{2.51}{Re*\sqrt{f(i+1)}}\right)}\right)^2 \\ f(i+3) &= \left(\frac{1}{\left(\frac{-2*\ln\frac{eps}{D}}{3.7}\right)+\left(\frac{2.51}{Re*\sqrt{f(i+2)}}\right)}\right)^2 \end{aligned} \tag{4.2}$$

where $f(i+1)$ is the first friction factor value based on the guess, eps is the pipe equivalent roughness for the SS-316 used in this project, and Re is the Reynolds number. $f(i+1)$ is used to determine $f(i+2)$, which is used to determine $f(i+3)$. The iteration process in Equation 4.2 ends when $f(i+n)$-$f(n)$ becomes negligibly small. When the changes in the friction factor become negligible small, Equation 4.1 becomes 4.3.

$$v = \sqrt{\frac{(P - P_{amb})}{\rho_{avg} * \left(\frac{\alpha}{2} + 0.5 * (k_c + f * \frac{L}{D}\right)}} \tag{4.3}$$

If the predicted exit velocity exceeds the choke flow velocity, the final predicted exit velocity becomes the choke flow velocity. As the blowdown continues and the RPV pressure decreases, the predicted velocity from Equation 4.3 decreases. If the value from Equation 4.3 is lower than the choke flow velocity, the final predicted exit velocity becomes the values from Equation 4.3.

Once the exit velocity is determined, the mass flow rate is determined by Equation 4.4:

$$\dot{m} = \rho v A \tag{4.4}$$

where $\dot{m}$ is the mass flow rate value exiting exiting the RPV, ρ is the density of the gas in the RPV, v is the velocity of the gas exiting the RPV, and A is the cross sectional area of the exit orifice in the RPV. The amount of mass exiting the RPV every time step is determined by Equation 4.5:

$$dm = \dot{m} * dt \tag{4.5}$$

where dm is the amount of mass exiting the RPV every time step and dt is the time step of the simulation. The new density in in the RPV is determined by Equation 4.6:

$$\rho(i+1) = \rho(i) - \frac{\dot{m} * dt}{V} \tag{4.6}$$

where $\rho(i+1)$ is the next calculated density in the RPV, $\rho(i)$ is the gas density of the RPV at iteration i, and V is the volume of the RPV.

Each iteration includes calculations for the temperature of the gas in the RPV and the RPV's wall temperatures. The equation for the temperature of the gas inside the RPV is determined with Equation 4.7:

$$T_g(i+1) = \frac{dt * h * SA}{c_v * m * T_w + (1 - dt * (\frac{h*SA+\dot{m}*R}{c_v*m}))} * T_g(i) \tag{4.7}$$

where $T_g(i+1)$ new gas temperature value being calculated for, h is the heat transfer coefficient in $\frac{W}{m^2K}$, SA is the surface area of the RPV, c_V is the specific heat capacity under constant volume for helium in $\frac{J}{KgK}$, T_w is the RPV wall temperature in Kelvin, and $T_g(i)$ is the gas temperature at the current iteration. The wall temperature is calculated by Equation 4.8:

$$T_w(i+1) = dt * 0.066 * P_0 * \frac{i * dt + (dt^2)^{-0.2}}{\rho_w * V_w * c_w} + \frac{dt * h * SA}{\rho_w * V_w * c_w} * T(i) + \frac{1 - dt * h * SA}{\rho_w * V_w * c_w} * T_w \tag{4.8}$$

where $T_w(i+1)$ is the new predicted wall temperature value, P_0 is the power generation, ρ_w is RPV's density, V_w is volume of the RPV structure, and c_w is the RPV's specific heat capacity.

The analytical solutions predicting the RPV blowdown pressure, the mass flow rate, and exit velocities during the blowdown are shown in Figures 4.4, 4.5, and 4.6. The code runs until the RPV pressure is within 100 pascals of atmosperic pressure. The code determined that these conditions were met at approximately 13.5 seconds.

The flowchart demonstrating the logical process of the entire calculation is shown in Figure 4.7.

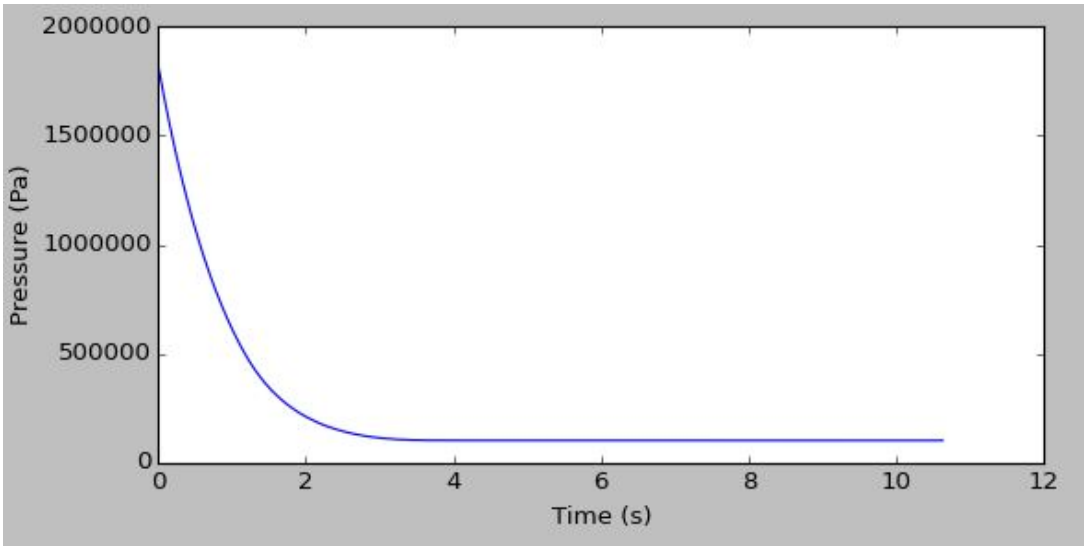

Figure 4.4: Predicted RPV pressure values from the python blowdown calculations with initial conditions set to 250 psig and 250 ° C.

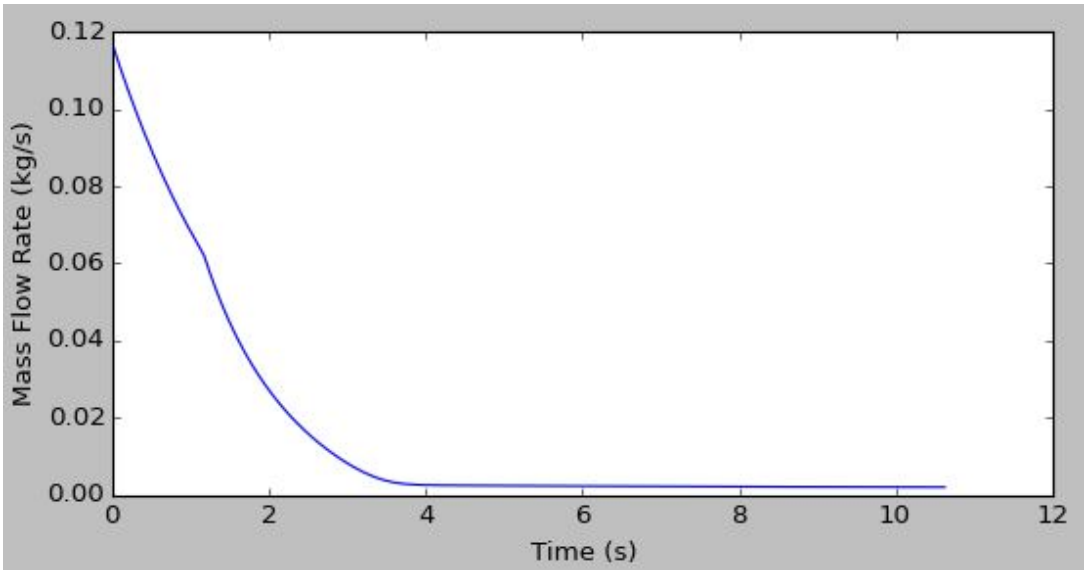

Figure 4.5: Predicted mass flow rate values from the python blowdown calculations with initial conditions set to 250 psig and 250 ° C.

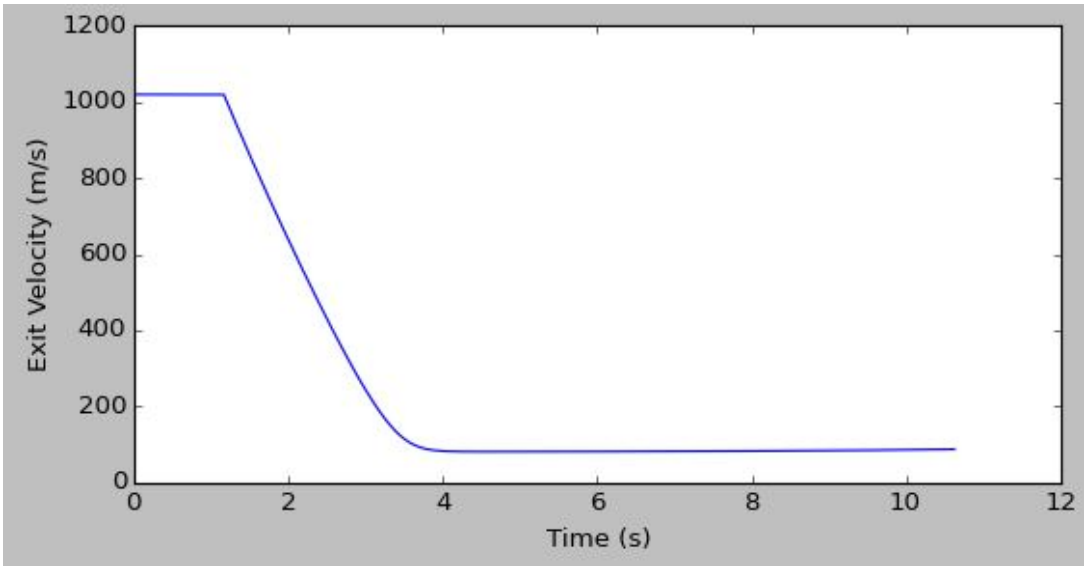

Figure 4.6: Predicted exit velocities from the python blowdown calculations with initial conditions set to 250 psig and 250 ° C.

Figures 4.4, 4.5, and 4.6 indicate that for the initial conditions of 250 psig and 250C, the analytical model predicts that most of the gas exits the RPV within 4 seconds following the blowdown's initiation. By applying different initial conditions, other blowdowns can be evaluated.

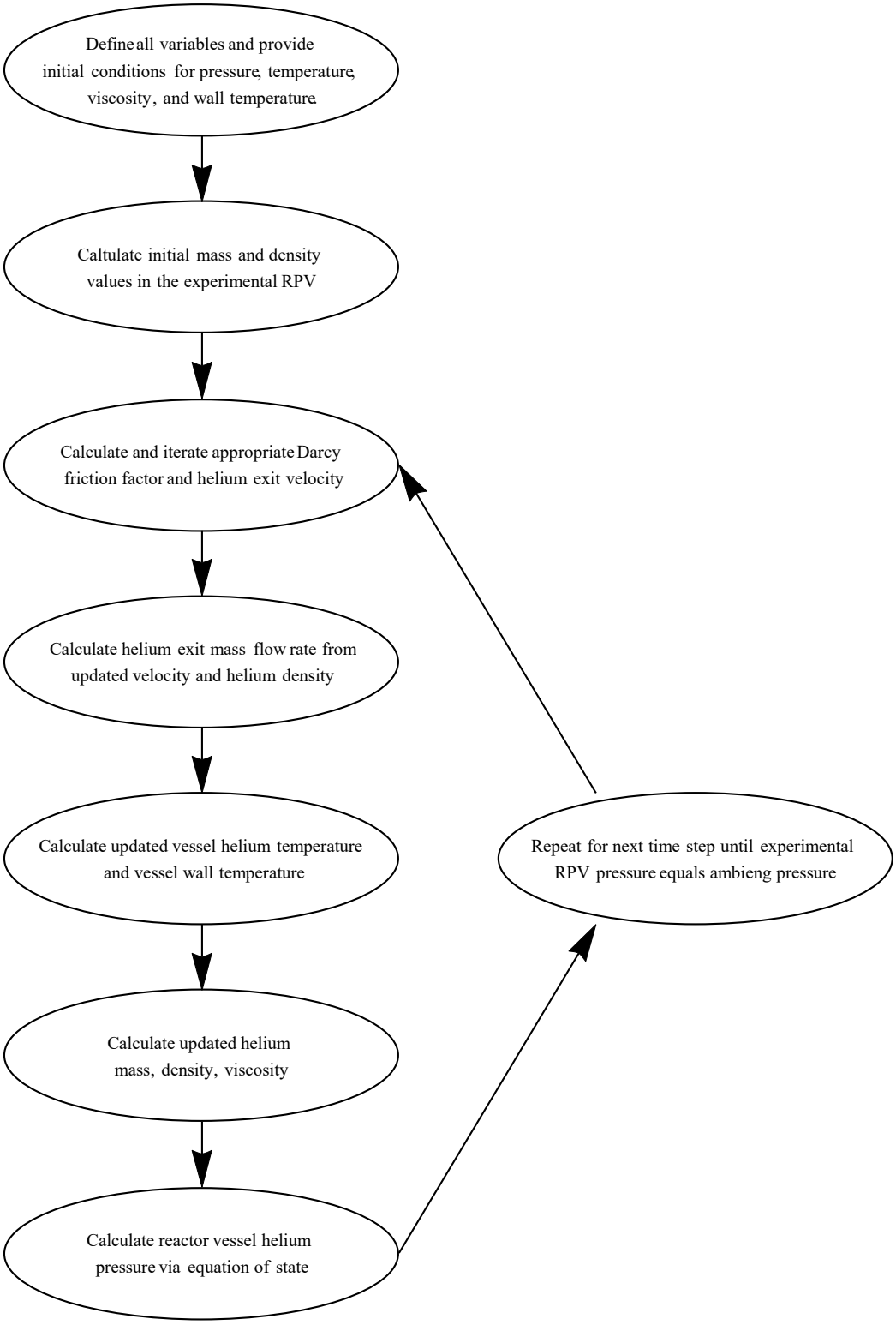

Figure 4.7: Flowchart demonstrating the logical process of the analytical solution.

CHAPTER 5

System Demonstration Results and Discussion

5.1 Introduction

This chapter first describes the placement of data acquisition instrumentation necessary to interpret the data. Next, data and analytical solutions are presented for three blowdown tests. The analytical solutions and acquired data are compared. These tests were performed and comparisons were made to demonstrate the viability of the apparatus. Plots of data are shown describing the gas mixing patterns, gas velocities inside the containment structure, RPV pressures, oxygen concentrations inside the containment structure, exiting gas temperatures in the ventilation port, and the temperatures inside of the RPV containment structure during the blowdown. Nitrogen was used in the first test. Helium was used in the two subsequent test. Analytical solutions are provided for the helium blowdown tests, and not for the nitrogen blowdown test.

5.2 Data Interpretation

This section provides necessary information to accurately interpret the data. It shows the thermocouple locations in the containment structure and the ventilation port, hot wire anemometers placement in the containment structure and ventilation port, and identifies the oxygen sensor's locations at different times during the blowdown.

5.2.1 Thermocouple Locations

The thermocouple locations inside of the containment structure are shown in Figures 3.10b, 3.21, 5.1, and 5.2. The thermocouples are held by swagelok fittings welded near the bottom of the windows. Six swagelok fittings are shown in Figure 5.1, showing the thermocouple locations on the front of the RPV containment structure. Six more swagelok

fittings, shown in Figures 3.21 and 5.2, are welded to the back of the RPV containment structure. The six thermocouple housings on the front and back of the RPV containment structure are located at identical heights.

Four thermocouples insert into the top plate of the containment structure. These thermocouple locations are shown in Figure 3.10b.

Four thermocouple locations are referred to in discussions about the blowdown phenomena later in thic chapter. These four locations are shown in Table 5.1. Table 5.1 also discusses their location on the RPV containment structure. Thermocouples attached to the top plate are referred to as either the "Containment Top", or "Top" location. Thermocouples at the bottom of the top window are referred to as the "Top Window" location. Thermocouples at the bottom of the middle window are referred to as the "Middle Window" location. Thermocouples at the bottom of the bottom window are referred to as the "Bottom" location. Table 5.1 also lists figures showing the thermocouple locations.

Table 5.1: Descriptions of the thermocouple placements in the containment structure.

Thermocouple Labels	Thermocouple Location	Reference Figure
Containment Top or Top	Top plate	3.10b
Top Window	Bottom of the top window	5.1 and 3.21
Middle Window	Bottom of the middle window	5.1 and 5.2
Bottom	Bottom of the bottom window	5.1 and 5.2

Five thermocouples are shown entering the ventilation port through swagelok fittings in Figure 5.3, behind the hot wire anemometers. They are labeled in the figure from left to right as 'TC3', 'TC2', 'TC1', 'TC4', and 'TC5'. All thermocouples are separated by two inches from each other. The two thermocouples near the ends of the ventilation port, TC3 and TC5, are 1 inch away from the sides of the ventilation port. Figure 5.4 shows the thermocouple and hot wire anemometer placement inside of the ventilation port.

Figure 5.1: Thermocouple locations, as indicated by blue arrows, in the RPV containment structure.

Figure 5.2: Thermocouple locations, as indicated by blue arrows, on the back side of the RPV containment structure.

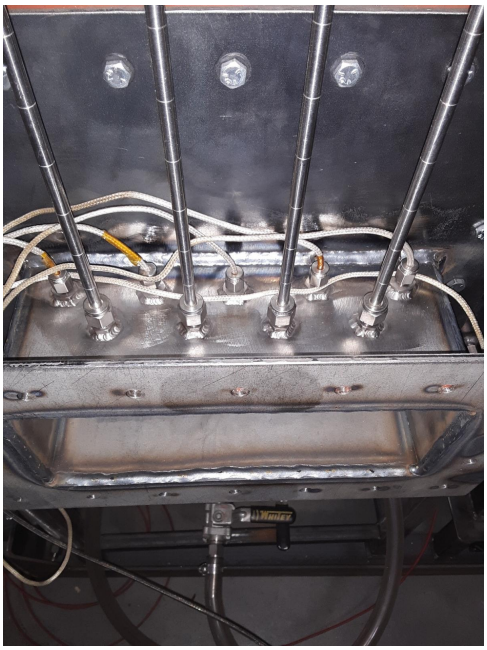

Figure 5.3: Swagelok fittings welded to the ventilation port to house the thermocouples and hot wire anemometers.

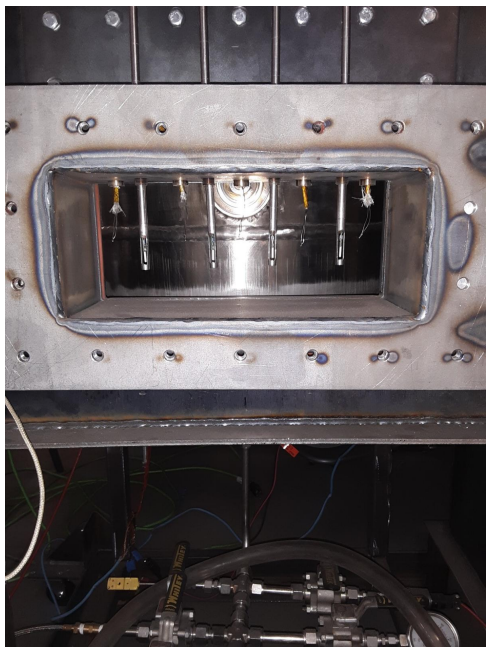

Figure 5.4: Thermocouples and hot wire anemometers inside of the ventilation port.

5.2.2 Hot Wire Anemometers Locations

Five hot wire anemometers are located in the containment structure and ventilation port. Four of these hot wire anemometers are shown in Figures 5.3 and 5.4. They measure the gas velocity as it exits the containment through the ventilation port. They are referred to, from right to left, as 'HW1', 'HW2', 'HW3', and 'HW4'. These hot wire anemometers are rated to measure gas velocities from 0-10.16 meters per second. [17]

The fifth hot wire anemometer is located inside of the containment structure, where it measures air velocities inside the containment during the blowdown. It can be placed in one of two locations. The first location, shown in Figure 5.5, is between the bottom and middle windows on the left side of the RPV containment structure. The second location, shown in Figure 5.6 is parallel to the top of the middle window of the RPV containment structure, just below the flange connecting the RPV containment structure to the top containment box. Figure 5.7 shows both hot wire anemometer housing locations in relation to each other, and in relation to other parts of the apparatus.

Figure 5.5: The hot wire anemometer housing on the left side of the RPV containment structure.

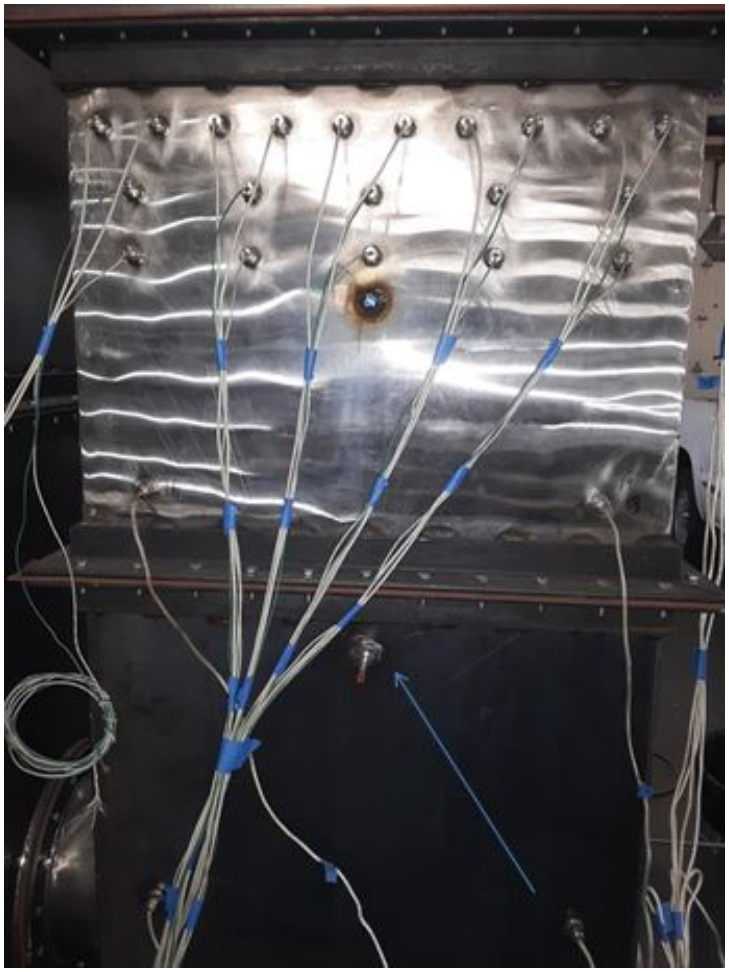

Figure 5.6: The hot wire anemometer housing, as indicated by a blue arrow, on the back side of the RPV containment structure.

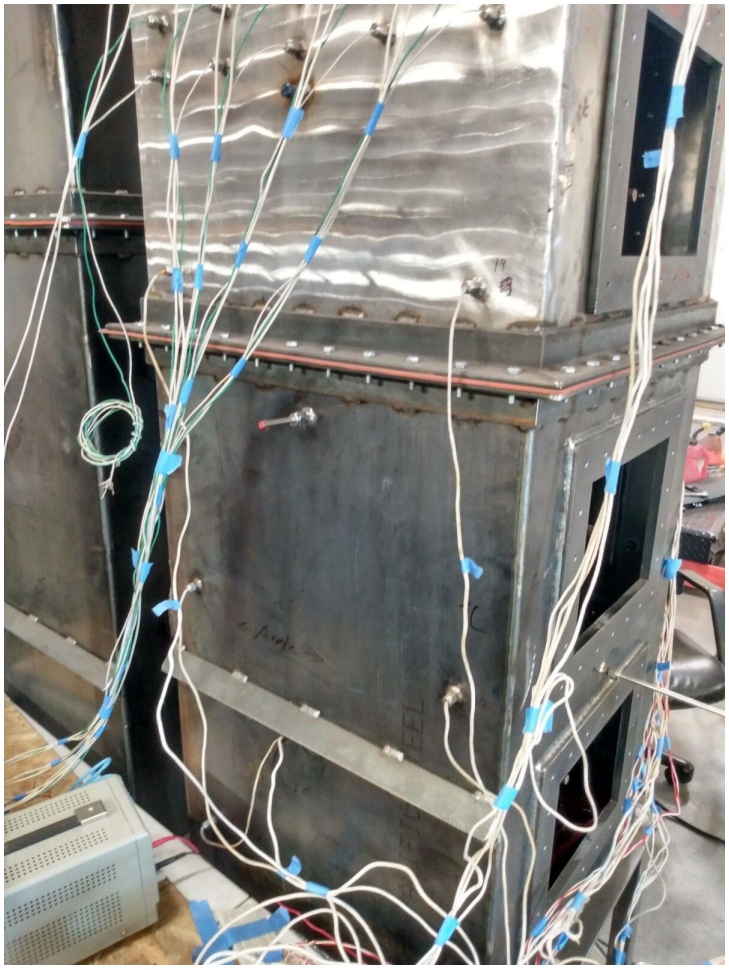

Figure 5.7: Both hot wire anemometer housings in relation to each other and in relation to other parts of the apparatus.

During all experiments discussed in this chapter, the hot wire anemometer in the containment structure was placed in the lower location on the left side of the containment structure, shown in Figure 5.5.

5.2.3 Oxygen Sensor

The oxygen sensor graphs show the oxygen concentrations plotted against time, as it is moving from the top of the containment structure to the bottom. Vertical lines are placed on the graph indicating the height of the oxygen sensor. The location of the line on the x-axis indicates the height of the oxygen sensor at a specific time.

5.3 Nitrogen Test

The first test was performed with nitrogen gas inside the RPV. Test parameters for the nitrogen blowdown are shown in Table 5.2. These initial conditions are achieved by pressurizing the RPV to 140 psig at room temperature. The heating cartridges were powered by Model TPC-1000 TEMPCO power controllers. These controllers provide 240 volts to the cartridges. The controllers were programmed to increase the cartridge temperatures 10° C per minute until they reached 250° C. By heating the gas in the RPV, the pressure of the gas increased from 140 psig to 250 psig. It took 90 minutes to heat the RPV to 250° C.The blowdown was initiated eight seconds after data acquisition began.

Table 5.2: Nitrogen blowdown test parameters.

Test Parameters	Values
Pre-Heat Pressure	140 psig
Experimental Temperature	250 ° C
Experimental Pressure	250 psig
Data Acquisition Rate	1 per second
Blowdown Location	Top-Front
Ventilation Location	Bottom-Front

Figures 5.8 through 5.12 show respectively the pressure decrease in the RPV, the velocity of gas exiting the containment structure, the oxygen concentrations inside the containment structure, the temperatures inside the containment structure, and gas temperatures exiting throgh the ventilation port during the blowdown.

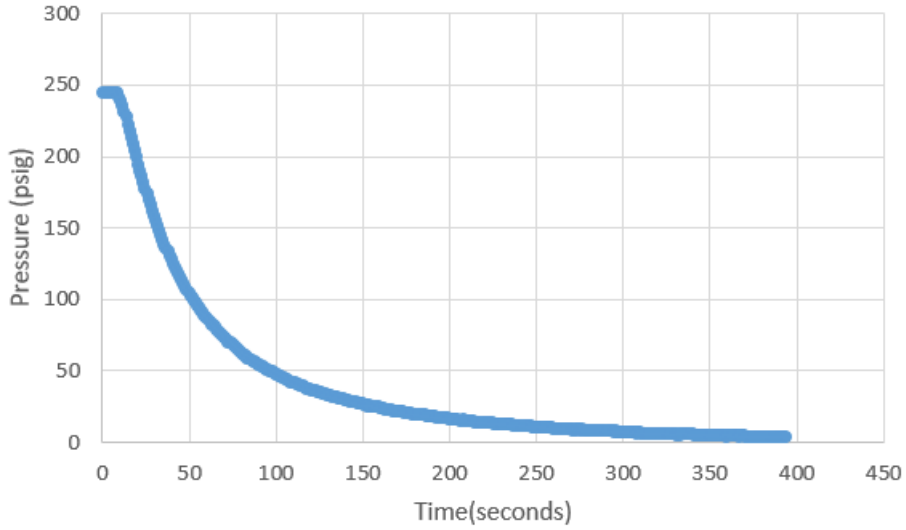

Figure 5.8: Gas pressure inside the pressure vessel during the nitrogen blowdown at 250° C.

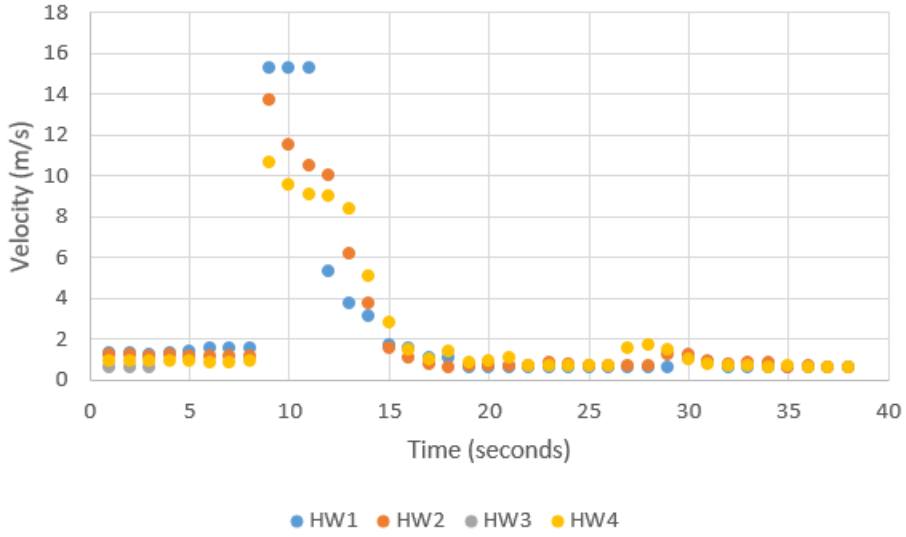

Figure 5.9: The combined plots of the hot wire anemometers readings on the ventilation port during the nitrogen blowdown at 250° C.

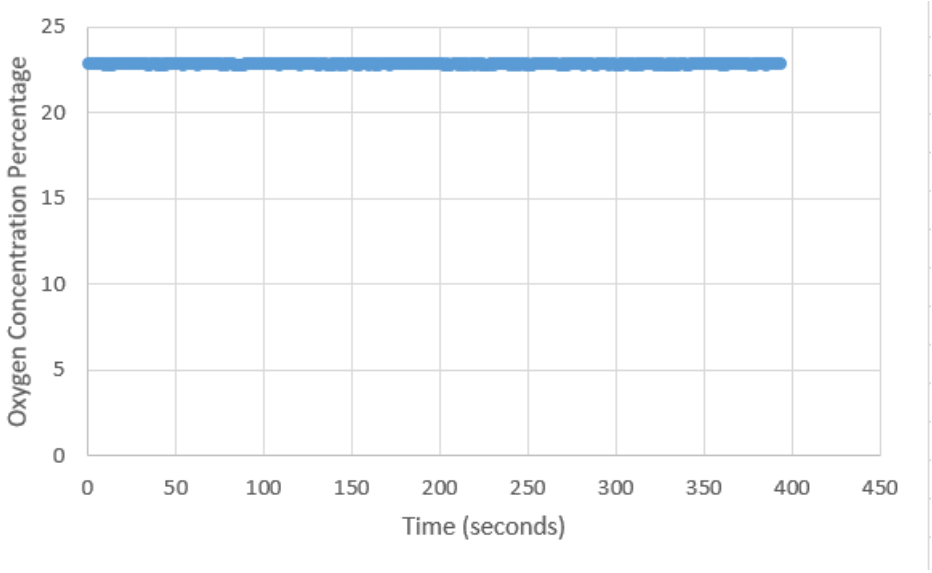

Figure 5.10: Oxygen concentration at different times during the nitrogen blowdown at 250° C.

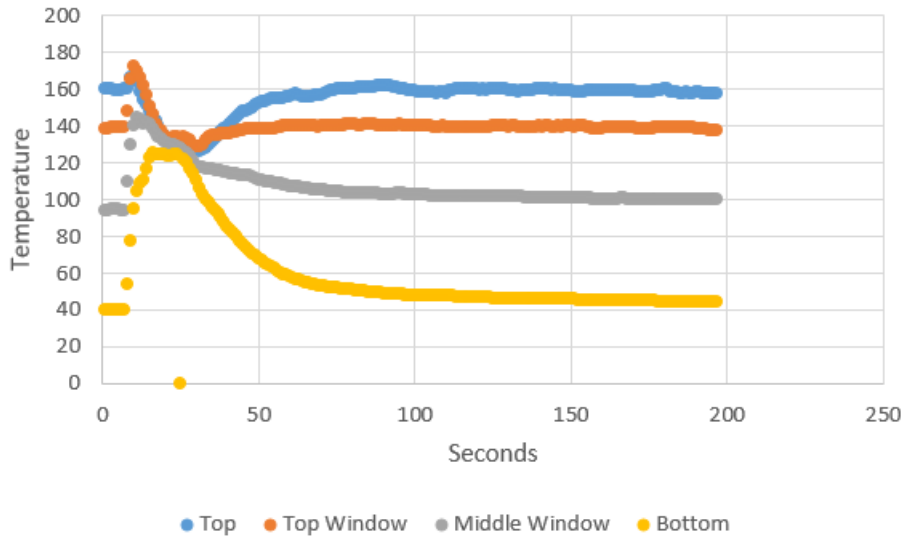

Figure 5.11: Temperatures during the Nitrogen blowdown event at 250° C.

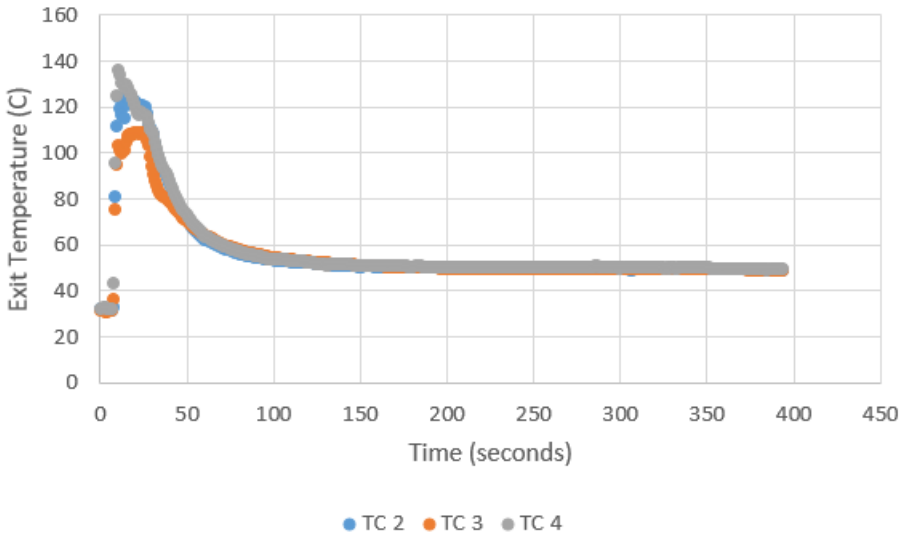

Figure 5.12: Thermocouple data inside the containment structure during the 250° C Nitrogen helium blowdown.

Figure 5.8 indicates that it took between 350-400 seconds for the RPV to blowdown close to atmospheric pressure.

Figure 5.9 shows that the velocity of the gas exiting the ventilation port reached approximately 15 meters per second within one second of initiating the blowdown. The exit velocities decreased to a very minimal velocity approximately 8 seconds after the blowdown's initiation.

Figure 5.10 shows that the oxygen concentration did not change over the course of the blowdown. It also suggested that the oxygen concentration values inside the containment structure were approximately 23%, which is highly unlikely. This indicates that the oxygen sensor failed to accurately acquire data during the nitrogen blowdown, or it was not calibrated accurately.

Temperature readings in Figure 5.11 show a temperature gradient of 120°C inside the containment prior to the blowdown. When the blowdown is initiated, the thermocouple readings merge together at approximately the 130° C. This is an indication of more or less complete mixing within the containment structure. A well mixed volume is further

indicated by Figure 5.12, wherein the exhaust temperature is approximately 130° C. It is also an indication of the temperature of the nitrogen gas as it exits the RPV. After about 75 seconds, the thermocouple values inside the containment structure returned to the temperature values prior the blowdown. The temperature readings in the ventilation port did not return to their initial values. They decreased to approximately 50°C.

The hot wire anemometer placed to read the air velocity inside the containment failed to acquire accurate data. Its failure is likely due to overheating. Because the instrument failed, its data is not included in this thesis.

5.4 Helium Test at Room Temperature

This section discusses the second blowdown test. It presents theoretical results from python and the data acquired from test results. This test was performed with helium. Its initial conditions are shown in Table 5.3. The blowdown was initiated approximately 10 seconds after data acquisition began.

Table 5.3: Test parameters for the helium blowdown at room temperature.

Test Parameters	Values
Experimental Temperature	20° C
Experimental Pressure	140 psig
Data Acquisition Rate	5 per second
Blowdown Location	Top-Front
Ventilation Location	Bottom-Front

5.4.1 Theoretical Blowdown Values from Python Calculations at Room Temperature

The predicted blowdown pressure, mass flow rate, and RPV exit velocity values are shown in Figures 5.13, 5.14, and 5.15. The Python code to determine the analytical solutions stopped when the pressure in the RPV was within 100 pascals of atmospheric pressure.

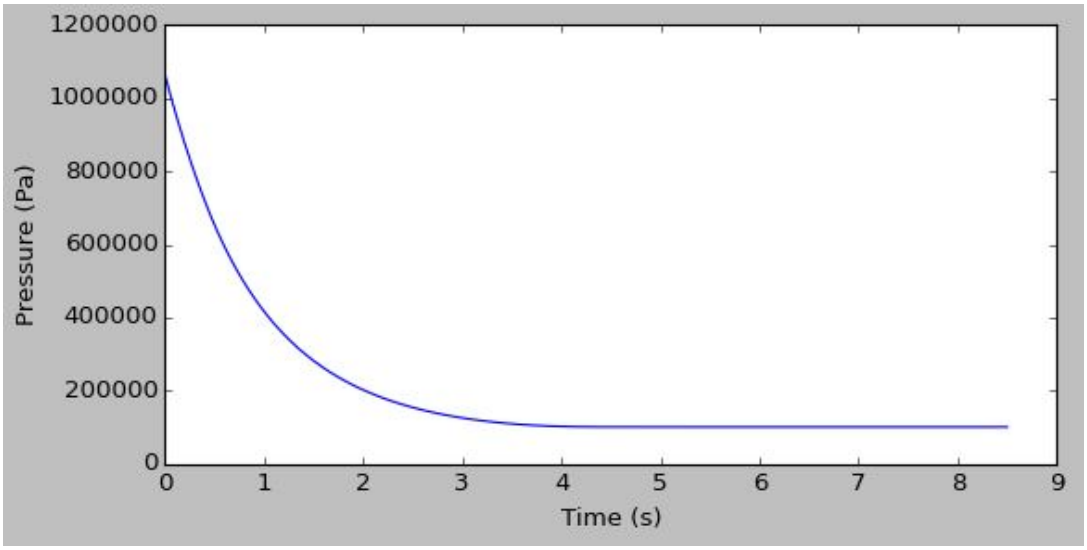

Figure 5.13: Predicted RPV pressure values from the python blowdown calculations with initial conditions set to 140 psig and 27° C.

The code predicted these conditions would be achieved at approximately 8.5 seconds.

Figures 5.13, 5.14, and 5.15 show the predicted time frame of the blowdown, the RPV's pressure, the mass flow rate, and the velocity of the gas exiting the RPV for the blowdown at 140 psig. The pressure values and mass flow rate curves in Figures 5.13 and 5.14 follow similar shapes. They both indicate that the majority of the helium gas will evacuate the RPV within about 4-5 seconds after the blowdown was initiated. The analytical predictions suggest that the blowdown at 250° C and 250 psig will be about 8 seconds longer than the blowdown at 27° C and 140 psig.

5.4.2 Helium Test at Room Temperature Blowdown Results

Figures 5.16 through 5.21 show the depressurization of the RPV, the velocity of gases inside the containment, the velocity of gases exiting the ventilation port, the oxygen concentration, the gas temperatures inside the containment, and the gas temperatures exiting the ventilation port.

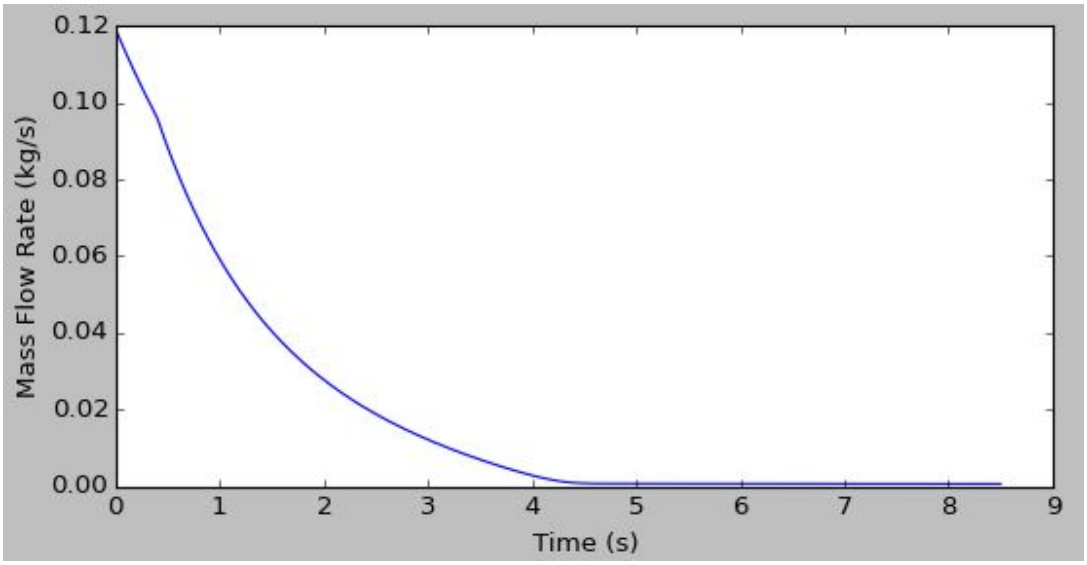

Figure 5.14: Predicted mass flow rate values from the python blowdown calculations with initial conditions set to 140 psig and 27° C.

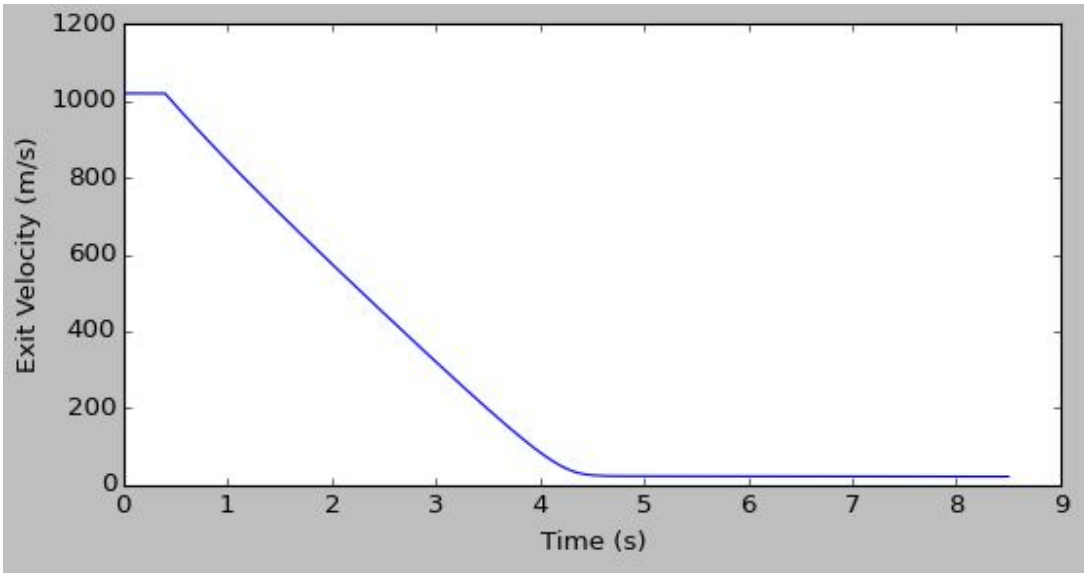

Figure 5.15: Predicted exit velocities from the python blowdown calculations with initial conditions set to 140 psig and 27° C.

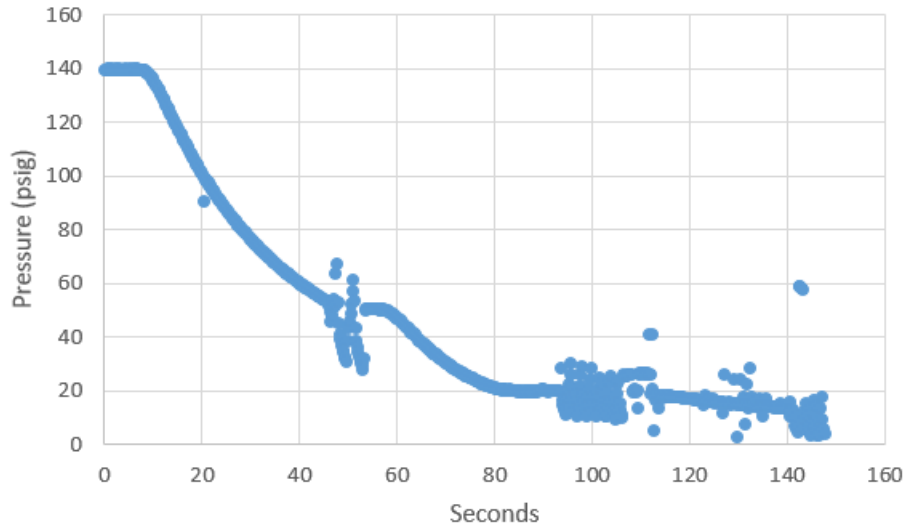

Figure 5.16: The pressure decrease during the helium blowdown at room temperature.

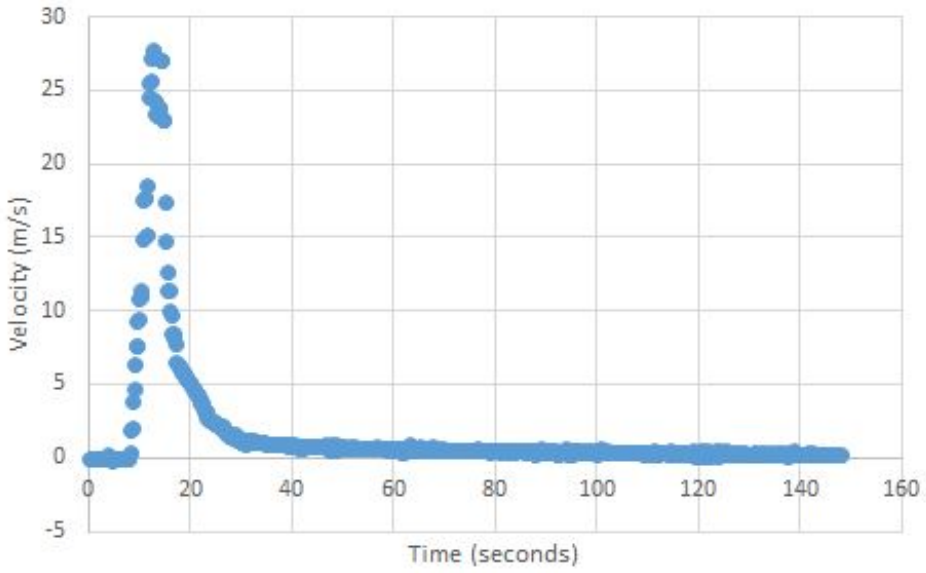

Figure 5.17: The gas velocity inside of the containment during the helium blowdown at room temperature.

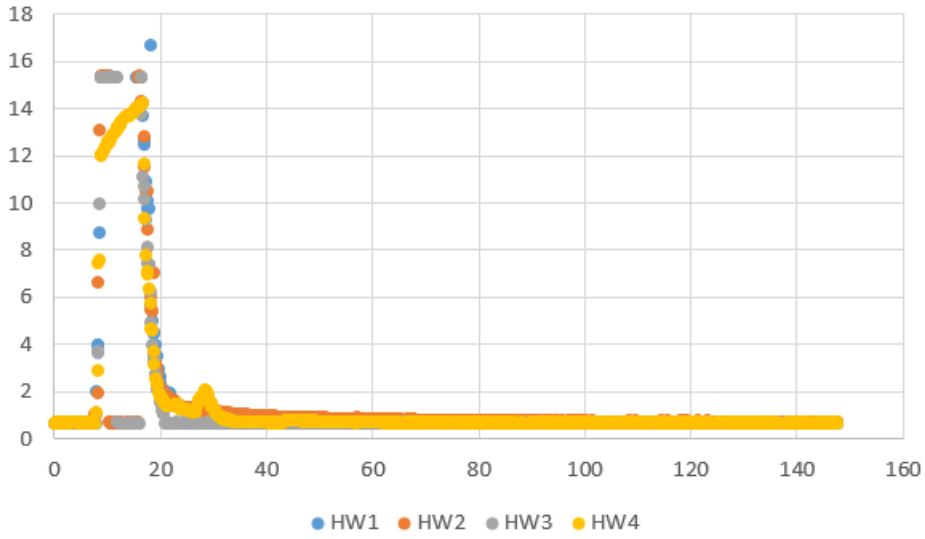

Figure 5.18: Combined hot wire anemometer plots of gas exiting the containment during the helium blowdown at room temperature.

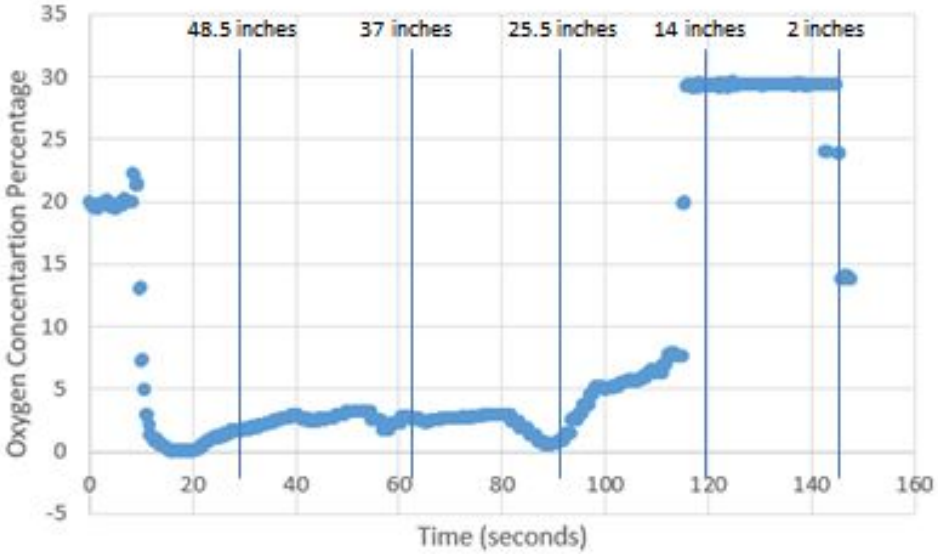

Figure 5.19: Oxygen concentrations following the helium blowdown at room temperature. Vertical lines indicate the height of the oxygen sensor at different times.

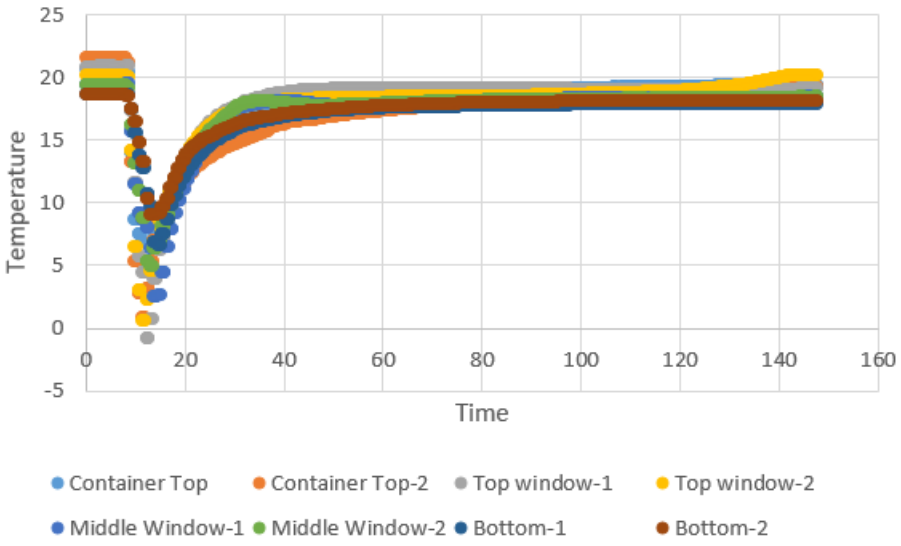

Figure 5.20: Temperatures of the gases mixing in the containment during the room temperature helium blowdown.

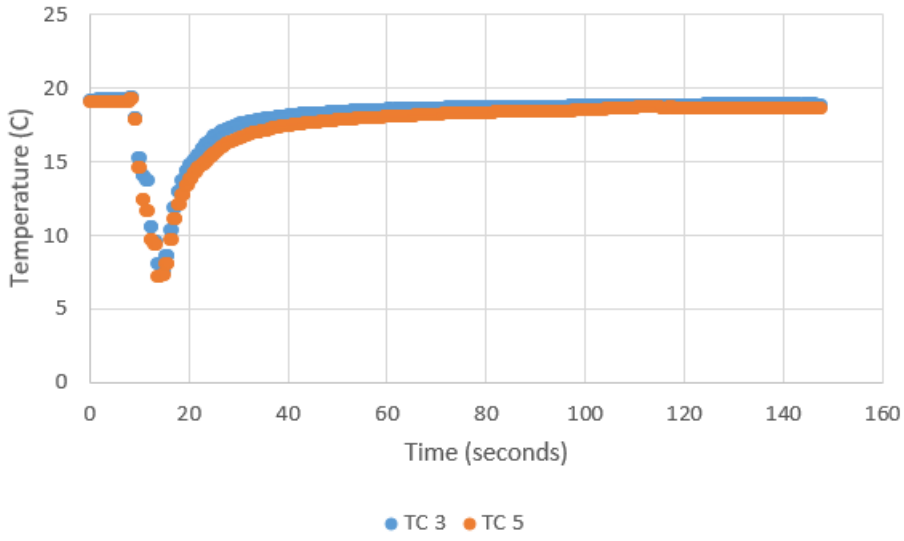

Figure 5.21: Temperature of the gas exiting the containment during the room temperature helium blowdown.

Figure 5.16 suggests that the blowdown at room temperature occurred almost entirely within 150 seconds. Around 30-40 seconds after initiating the blowdown, the pressure stayed level for a span of nearly 10 seconds. The reason for this momentary pressure stabilization might be due to the increase of the pressure in the containment structure.

Figure 5.16 shows that the final pressure of the RPV was 14 psig. Closing the ventilation port door prematurely prevented the system from completely depressurizing.

Figure 5.17 suggests that the gases move at the highest velocities within the first 10 seconds of the blowdown. After 10 seconds, the gases still move, but at significantly lower speeds. This pattern is also demonstrated in Figure 5.18, which shows the combined hot wire anemometer measurements of the gases exiting the ventilation port. Similar to Figure 5.17, the data suggests that the highest gas velocity occurs in the first 10 seconds of the blowdown.

Figure 5.19 shows the oxygen concentration readings during the blowdown. After the blowdown was initiated, the oxygen sensor readings suggested oxygen concentrations between 2% and 4% for the first 90 seconds of the blowdown. Approximately 90 seconds after the blowdown was initiated, the oxygen concentrations began to rise. Approximately 115 seconds after the blowdown was initiated, the oxygen sensor failed, indicating oxygen concentration values of 30%. The oxygen sensor seemed to function correctly shortly before the end of data acquisition and read a concentration at the bottom of the containment structure of approximately 13%. This oxygen concentration is similar to the oxygen concentration value at the bottom of the containment structure during the blowdown at 140° C.

The data shown in Figure 5.20 shows a temperature gradient of about 5° C from the top of the containment structure to the bottom. When the blowdown is initiated, all thermocouple readings in the containment, including the ventilation port temperature readings shown in Figure 5.21 decrease by approximately 10-20° C. Temperatures in the containment structure and ventilation port return close to ambient temperatures values within approximately 30 seconds after the blowdown, but don't reach the same temperatures prior to the blowdown.

The analytical solutions suggest that this blowdown should be mostly finished ap-

proximately 8.5 seconds following the blowdown. Actual blowdown data shows that the blowdown takes longer than the analytical solution predicts. This difference exists in part because the analytical solution does not account for the friction between the gas and the containment structure or the pressure build up inside the containment following the blowdown. Within 5-10 seconds after initiating the blowdown, the experimental data shows the gas velocities in the containment hit a maximum value and return to negligible values. The temperatures in the containment structure and ventilation port decrease by about 10-20° C within about 10 seconds of the blowdown and return close to their original values nearly 30 seconds after the blowdown was initiated.

5.5 Helium Test at 140° C

This section discusses the third preliminary blowdown test. It presents theoretical results from python and the data acquired from test results. The test was performed with helium. Its initial conditions are shown in Table 5.4. The blowdown was initiated approximately one second after data acquisition began.

Table 5.4: Test parameters for the helium blowdown at 140° C.

Test Parameters	Values
Pre-heat Pressure	140 psig
Experimental Temperature	140° C
Experimental Pressure	200 psig
Data Acquisition Rate	5 per second
Blowdown Location	Top-Front
Ventilation Location	Bottom-Front

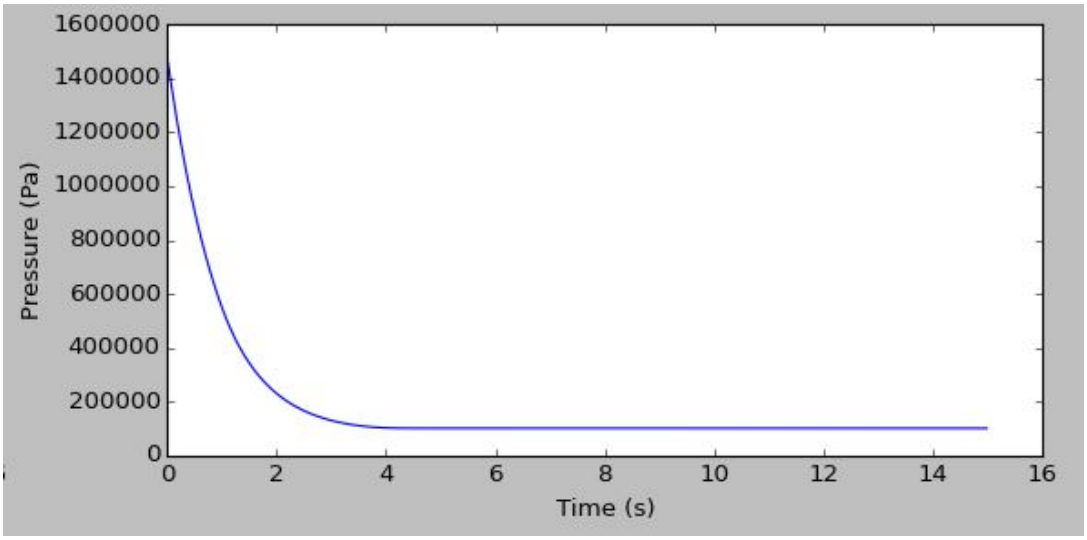

Figure 5.22: Predicted RPV pressure values from the python blowdown calculations with initial conditions set to 200 psig and 140°C.

5.5.1 Theoretical Blowdown Values from Python Calculations at 140°C

The predicted blowdown pressure, mass flow rate, and velocity values are shown respectively in Figures 5.22, 5.23, and 5.24. The Python code to determine the analytical solutions stopped when the pressure in the RPV was within 100 pascals of the atmospheric pressure. The code predicted these conditions would be achieved at 15 seconds.

The analytical solutions for the blowdown at room temperature and the blowdown at 140°C show very similar shapes. Even though they are very similar, there are several differences between the graphs of the two blowdowns. Analytical solutions suggest that the choked flow time during the blowdown at 140°C lasted approximately 0.5 seconds longer than the blowdown at 27°C. The pressure and mass flow rate graphs similar shapes, but RPV depleted to within 100 pascals approximately 6.5 seconds faster in the 27°C predicted solution than the 140°C predicted solution.

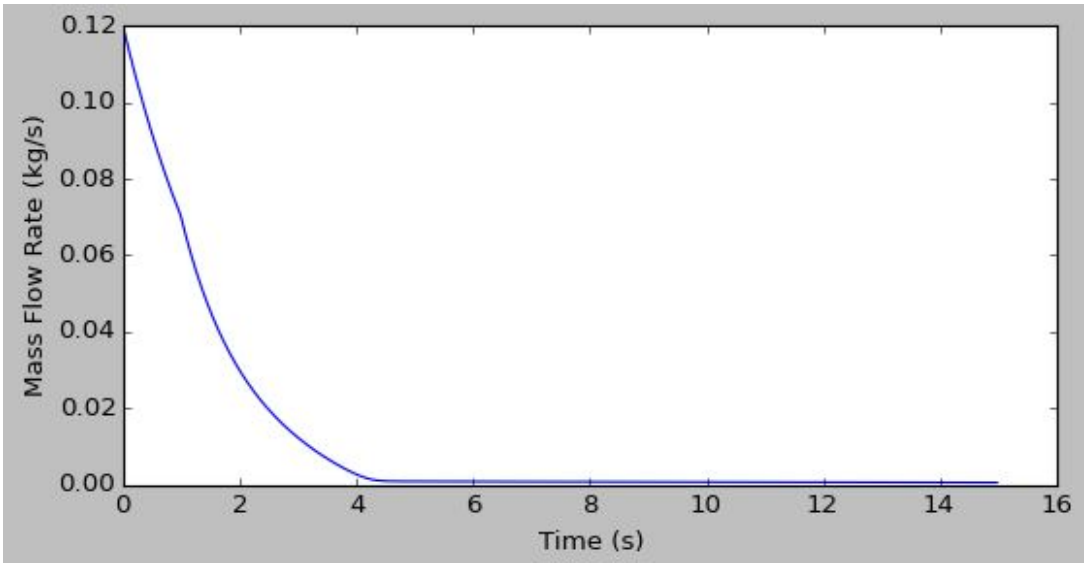

Figure 5.23: Predicted mass flow rate values from the python blowdown calculations with initial conditions set to 200 psig and 140°C.

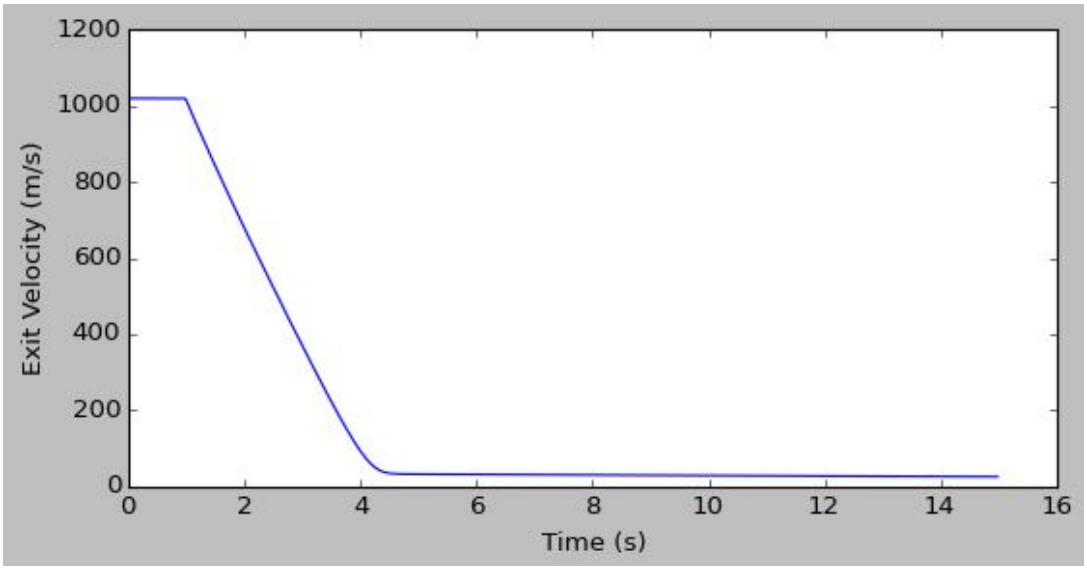

Figure 5.24: Predicted exit velocities from the python blowdown calculations with initial conditions set to 200 psig and 140°C.

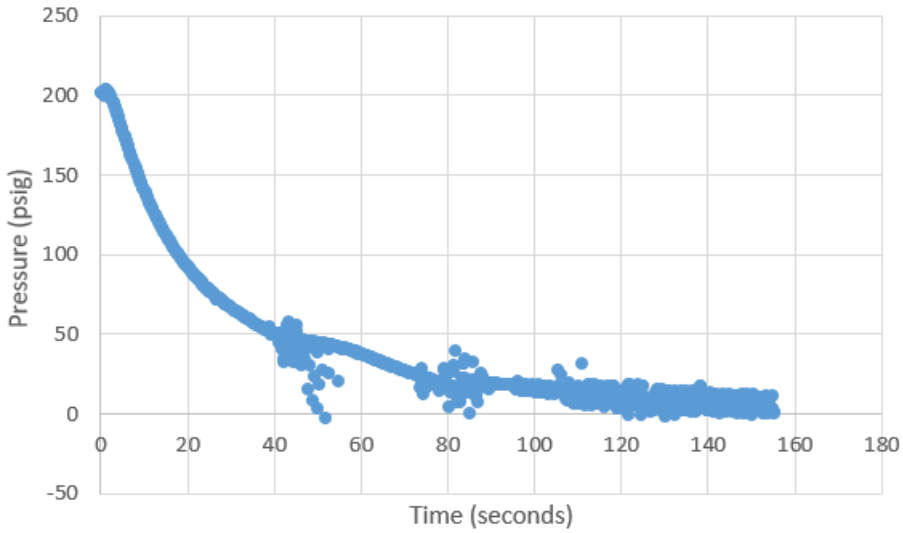

Figure 5.25: The depressurization of the 140° helium blowdown.

5.5.2 Helium Test at 140°C Blowdown Results

Like the nitrogen blowdown, the RPV was pressurized to 140 psig before the gas was heated. Three cartridges were heated by 120V variacs. Unlike the Tempco power controllers, the variacs could not be programmed to increase temperature based on the thermocouple values inside of the heating cartridges. They provide a constant power supply regardless of the temperature of the cartridge. A fourth cartridge was powered by a Model TPC-1000 TEMPCO power controller which provided 120 volts. This power controller cannot heat a cartridge above 100°C. After the system was heated, the pressure of the gas inside the cylinder reached 200 psig. Figures 5.25 - 5.29 depict the RPV's pressure, the gas velocities exiting the containment, the oxygen concentration in the containment, the gas temperatures inside the containment, and the gas temperatures exiting the ventilation port during the blowdown.

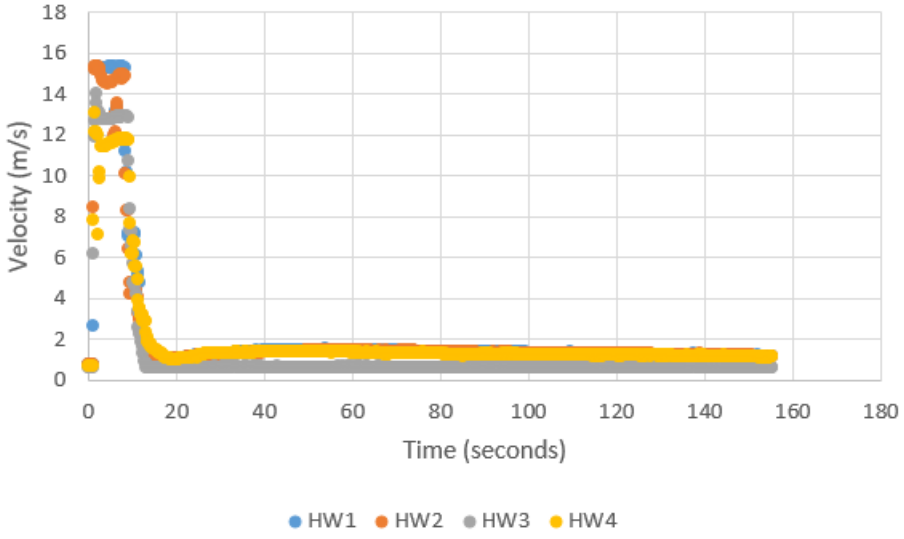

Figure 5.26: The gas velocities exiting the ventilation port during the 140° helium blowdown.

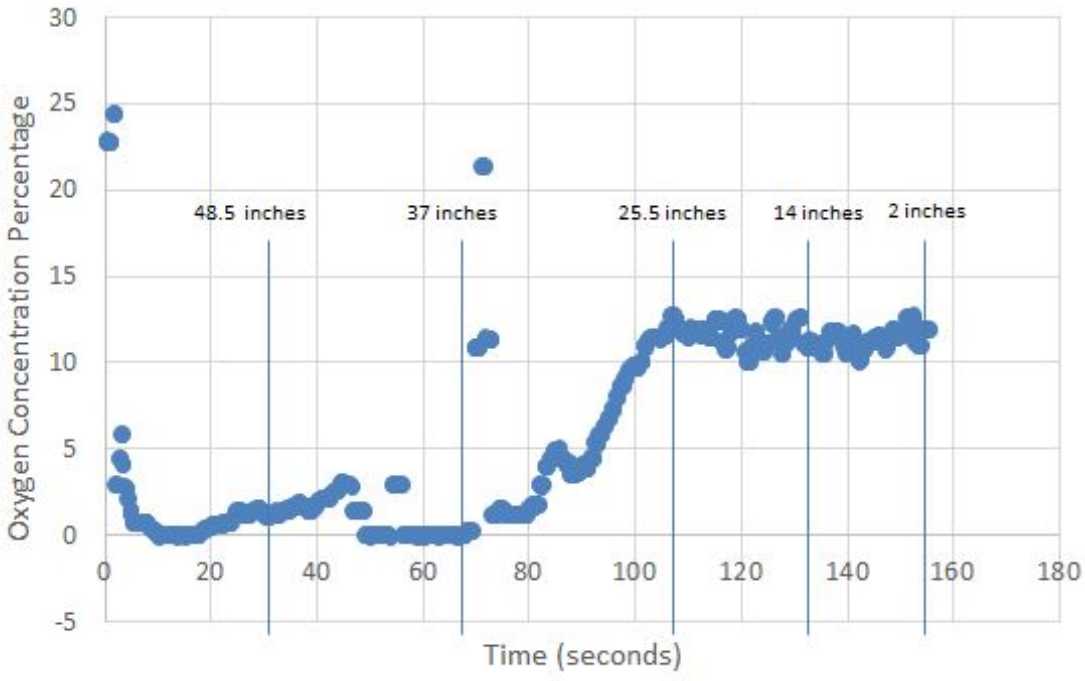

Figure 5.27: Oxygen concentrations following the 140° C helium blowdown. Vertical lines indicate the height of the oxygen sensor at different times.

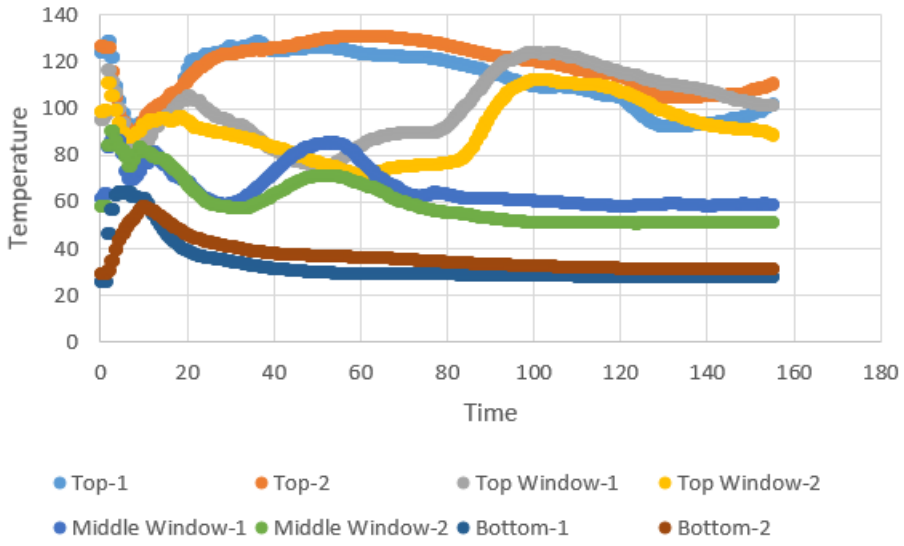

Figure 5.28: Temperatures of the Helium blowdown at 140° C.

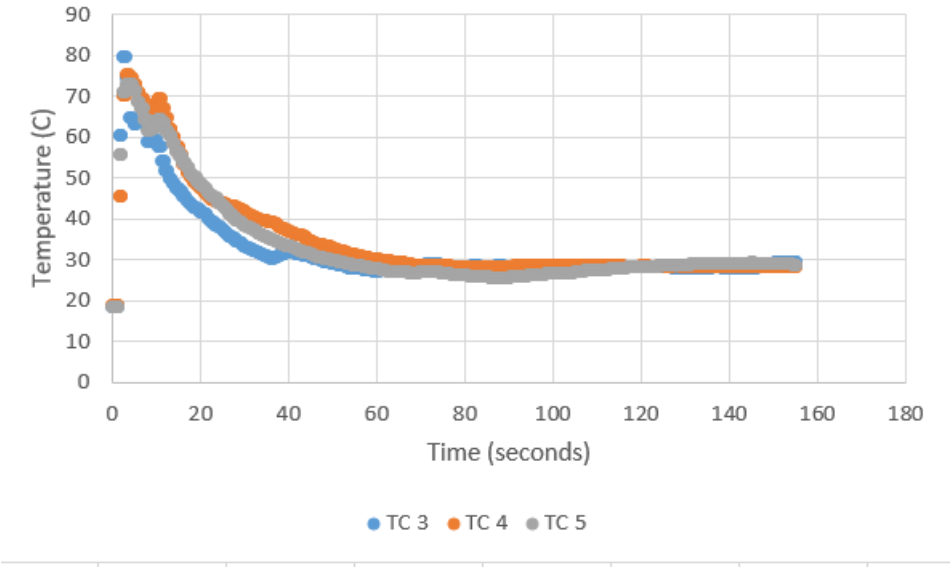

Figure 5.29: Temperature of the gas exiting the containment during the 140° C helium blowdown.

The data collected by the high velocity hot wire anemometer measuring the velocity of the gases inside the RPV containment structure is not shown. Similar to the first heated blowdown with nitrogen, it failed, likely due to excessive heat exposure from the RPV.

Figure 5.25 shows that the blowdown at 140°C took approximately 155 seconds. The

RPV's pressure started to level for a brief moment around 40-50 seconds, similar to the blowdown at room temperature.

Figures 5.28 and 5.29 show that the temperatures began to converge to an average value of about 75°C. Unlike the nitrogen blowdown tests, the thermocouple readings did not completely converge. This further confirms a well mixed system during the blowdown.

Unlike the first blowdown with nitrogen, Figure 5.27 suggests the blowdown with helium caused a significant change in oxygen concentration inside the RPV containment. The graph depicts the oxygen in the top half of the containment structure to be almost depleted shortly after the entire blowdown was initiated. At around 70 seconds after data acquisition, the oxygen sensor readings began to indicate a rise in oxygen concentration. During this time, the oxygen sensor was being lowered from 37 inches to 25.5 inches. The oxygen concentration reached its maximum of about 12.5% at around 105 seconds when the oxygen sensor was moved to 25.5 inches. The oxygen concentration stayed near this same value for the rest of data acquisition. The increase of oxygen concentration readings from 70-105 seconds gives some understanding of when the oxygen sensor was surrounded primarily by helium gas, primarily air, or a mix of the two gases.

The oxygen sensor was most effective in reading oxygen concentrations during this blowdown than the others. The data was continuous and did not suggest unrealistic oxygen concentration values.

The temperature data inside of the containment suggests a 100°C temperature gradient from the top to the bottom of the RPV containment structure. After the blowdown was initiated, the gradient decreased to about 30°C. The temperatures in the upper half of the containment did not return to their original values. This could be an indication of movement of the gases within the containment structure. This is the area where CFD calculations would be very instructive. At the end of data acquisition, the stratification is generally what would be expected. A temperature gradient similar to the initial

temperature gradient is found. The temperatures in the lower half of the containment returned to their original values within about 80 seconds after the blowdown.

The analytical solutions suggest that the 140°C blowdown should be mostly finished within 15 seconds after the initiation of the blowdown. Actual blowdown data shows that the blowdown takes longer than the analytical solution predicts. This is expected because the analytical solution does not take into account the additional volume of the containment nor the friction encountered by the exiting gas. Within 15-20 seconds after initiating the blowdown, the experimental data shows the gas velocities exiting the ventilation port reach a maximum value and return to negligible values. The change of temperatures in the containment structure and the ventilation port all occur within the same 15-20 second range. The time scale of the analytical solution is generally shorter that the actual blowdown for the reasons explained earlier. The analytical solution does give a lower bound of the actual blowdown time scale.

5.5.3 Data Comparisons

In comparing the analytical solutions and experimental results, there seems to be two common trends noticed. First, acquired data indicates that the majority of the helium/air mixing phenomena and depressurization of the RPV happen within the first 15-25 seconds after initiating the blowdown. Second, the analytical solutions predict that the blowdown phenomena occurs significantly faster than the acquired data indicates. Even though there is a significant difference in the predicted time from the analytical solutions and the acquired data, they both indicate that the majority of the helium exiting the RPV and mixing occurs in the preliminary stages of the blowdown.

CHAPTER 6

Conclusions and Future Work

6.1 Introduction

The apparatus was tested with three blowdown tests. Each test varied in either the type of gas inside the RPV, the pressure, or the temperature of the RPV. This section discusses what was learned from these tests and what future work should be done to improve the apparatus. These improvements will increase understand of the helium/air mixing patterns inside of the containment structure of a VHTR following a LOCA.

6.2 Conclusion and Instrumentation Analysis

This section discusses the effectiveness of the pressure transducer, oxygen sensor, hot wire anemometers, and thermocouples.

6.2.1 Pressure Transducer

The pressure transducer was the most effective and consistent data acquisition instrument. It consistently produced continuous data without major glitches. It proved to be effective at the temperatures and pressures of all three blowdown tests.

6.2.2 Oxygen Sensor

The oxygen sensor was most effective during runs at lower temperatures. During the Nitrogen blowdown when the pressure vessel was heated to 250°C, the oxygen completely failed to determine of oxygen concentration variations as it was moved from the top of the containment to the bottom. The data also suggests that the oxygen concentrations in the containment exceeded 20%, which is not possible. It inaccurately read oxygen

concentrations at the end of the room temperature blowdown. Data in figure 5.19 shows that between time 115 and 145, the oxygen concentration inside the RPV containment was nearly 30%, which is also not possible.

The oxygen sensor shaft was effective in moving the oxygen sensor mounting bracket to different heights in the RPV containment structure. It was difficult to consistently determine the height of the mounting bracket. For this reason, oxygen concentrations at different heights were not known specifically.

6.2.3 Hot Wire Anemometers

The hot wire anemometers were mostly effective in obtaining consistent data. The high-velocity hot wire anemometer failed due to heat exposure during both heated test. It effectively collected data during the blowdown at room temperature.

The effectiveness of the hot wire anemometers in the ventilation port was questionable in two circumstances. First, they indicated air velocities higher than what they were rated for. Second, they plateaued during several tests. The hot wire anemometers in the ventilation port are further away from the RPV than the high velocity hot wire anemometer. For this reason, it is not likely that their effectiveness was compromised due to RPV proximity.

-

6.2.4 Thermocouples

There are 16 thermocouples in the RPV containment structure and five thermocouples in the ventilation port. In the data showing the temperatures, there are never more than eight thermocouples readings reported for the containment structure and three for the ventilation port. This is because the insulation frayed during calibration and testing, which caused them to fail.

6.2.5 Blowdown Analysis via Instrumentation

In Chapter 2, the three sequential blowdown phases stated were forced convection, mixing, and stratification. This subsection identifies how these phenomena can be analyzed with the data acquired with the instrumentation.

Forced convection is indicated by the rapid increase of gas velocities in the containment structure and in the ventilation port. Velocity graphs are shown in in Figures 5.9, 5.17, 5.18, 5.26. Figure 5.18 best demonstrates forced convection by depicting the rapid increase of velocity in the containment structure within a few seconds after the blowdown was initiated. The gas velocities increased to nearly 27 $\frac{m}{s}$. According to the data, and the analytical solution, the majority of the helium evacuates the RPV within the first 20 seconds of the blowdown, and the entire blowdown is on the order of 150 seconds.

Gas mixing is indicated by the converging gas temperatures inside the containment structure following the blowdown. Converging temperatures in the containment are found in Figures 5.11, 5.12, 5.20, 5.21, 5.28, and 5.29. All of the previously stated figures show that temperatures completely converged or were beginning to converge after the blowdown was initiated. The gas mixing phase via forced convection time frame was within the first 15-20 seconds following the blowdown.

Stratification is indicated by the oxygen sensor reading. The oxygen sensor readings indicate the actual oxygen concentration levels in the gases. When zero oxygen percentage is indicated, the oxygen sensor is most likely surrounded by primarily helium. When oxygen concentration readings are above zero percent, the oxygen sensor is most likely surrounded by a mixture of helium and air. Oxygen concentration readings indicate stratification in the containment structure in Figures 5.19 and 5.27 by showing higher oxygen concentrations in lower portion of the containment structure than the top portion. From the oxygen sensor readings, it is evident that the time period of the stratification starts at 65 seconds and appears to be complete at 100 seconds.

6.3 Future Work

This section discusses future work related to data acquisition instrumentation and procedures, which will improve the design and effectiveness of the experimental apparatus.

6.3.1 Pressure Transducer

The pressure transducer provided the most consistent data of all the data acquisition instrumentation. It provided data on the pressure inside the RPV during the blowdown. Knowing the pressure inside the containment structure during the blowdow would provide valuable understanding of the gas patterns inside the containment structure during a blowdown. It would increase the understanding of oxygen concentration readings from the oxygen sensor because the oxygen sensor's readings are pressure dependent. An electronic pressure transducer should be attached to the containment structure to read its pressure during the blowdown. The range of the pressure transducer can be estimated by performing a blowdown experiment with a manual gauge attached to the containment structure and observing the maximum pressure on the manual pressure transducer.

6.3.2 Oxygen Sensor

In order to understand the data from the oxygen sensors, the exact position of the oxygen sensor needs to be known at all times. The NEMA-17 stepper motor was purchased from AdaFruit to turn the all thread. [21] When it was used, it failed to turn the all thread faster than two revolutions per second. The oxygen sensor cannot be moved manually during future blowdowns. It must be moved by a stepper motor. A stepper motor more powerful than the NEMA-17 is needed to turn the all thread. This will make it possible to know exactly where the oxygen sensor is at all times inside of the containment structure while also turning the all thread fast enough.

If the oxygen sensor fails during future blowdowns at 250°C, blowdown temperatures should be decreased. The oxygen sensor's data sheet says that is capable of functioning with gases up to 250°C and that it does not require stabilization based on varying temperatures. [16] Based on the data shown in Figure 5.8, the oxygen sensor failed at 250°C. The oxygen sensor should be tested to determine its maximum functional temperature.

The CFD predictions shown in Figures 4.3a and 4.3b give a clear indication that the line between the helium and air gas inside of the RPV containment structure is at the co-axial cross vessel between the two vessels. It allows helium to escape from the RPV containment to the PGV containment. This could be a good indication of the oxygen sensor's optimal placement prior to the blowdown. If the top half of the containment structure contains primarily helium and all the gas mixing is occurring in the bottom half of the containment, it might be most effective to focus primarily on oxygen concentrations near the co-axial cross vessel. This suggestion might only be applicable for blowdowns with the blowdown and ventilation ports in these locations. The line between helium and air could be in a completely different height based on the location of the blowdown and ventilation ports.

6.3.3 Hot Wire Anemometer

There are two possible options to resolving the issues discussed in section 6.2.3. The first is to calibrate them to the velocities they read in the experiment. If they prove capable of reading the data up to that range, they can be kept. If they fail during calibration at the velocities shown in the data, new hot wire anemometers need to be purchased that are rated for the velocities exiting the containment vent.

The heating issue with the hot wire anemometer inside the containment structure can only be resolved by changing the temperature of the blowdown. Experiments could be

performed at lower temperatures and varying pressures to determine the velocity of gases mixing in the containment structure.

6.3.4 Thermocouples

The fiberglass insulated thermocouples need to be replaced by rigid thermocouples. Stainless steel ferrules will create an air-tight seal around the metal sheath thermocouples. It will also significantly decrease the chance of the thermocouples from failing. Using metal sheath thermocouples will increase the data points in the apparatus and lead to a greater understanding of the heat transfer occurring in the containment structure.

6.3.5 Procedural Future Works

During the three blowdowns described in this thesis, the ventilation port was always closed 30 seconds after the blowdown was initiated. During future blowdown tests, the ventilation port should be kept open until the blowdown is entirely finished. According to the experiments discussed in this thesis, that time is approximately 150 seconds. Leaving the ventilation port open until the blowdown is finished might prevent issues like the one shown in figure 5.8, where the RPV never fully depressurized.

Performing the blowdowns described in Table 3.4 can provide valuable information about the helium/air mixing patterns inside the containment structure. They are not the only tests that can provide valuable information about gas mixing patterns. For example, placing the ventilation port on the bottom of the containment structure of the PGV could prove to be a valuable method of removing oxygen from the containment structure. As said earlier in this section, the pressures and temperatures of blowdown tests can be changed to be more compatible for instrumentation like the hot wire anemometer and oxygen sensor.

Before performing experiments in CAES, instrumentation should be re-calibrated.

This will ensure the functionality of all instrumentation was preserved while the system was being transported from the fabrication shop to CAES. It will also ensure the accuracy of the newly purchased instrumentation.

6.3.6 Future CFD Simulations

At various times and locations in the experiment, it is challenging to determine the phenomena occurring inside the containment structure. For example, thermocouple readings shown in Figure 5.28 indicate heat transfer is occurring at and above the top window location between the containment structure, the vessel and the enclosed gas. This is determined by the change in temperature values at the top window location between 80-100 seconds. In this time, the temperatures increased from 80°C to 110°C. Understanding of this type of phenomena would increase with further CFD simulation.

6.4 Input to the Nuclear Field and the Design of the VHTR

The scaled system will be used in further blowdown experiments to acquire data describing gas mixing patterns and phenomena following a blowdown of a VHTR. This data will be used by CFD computational scientists to run prototype-scale blowdown simulations. These CFD simulations, aided by experimental data acquired by blowdown tests with this scaled VHTR model, will help enhance the safety of the VHTR design and mitigate potential risks following a structural failure of a VHTR.

The impacts of increasing the security of individual reactor designs could reach beyond the way that reactor operators respond to failures. These impacts could extend to increasing the probability of nuclear power plants being developed and used to create energy by decreasing public fear of catastrophic events related to nuclear power plant failures.

Research presented and discussed in this thesis gives insight as to how the design of the

VHTR can help prevent oxygen ingress into the reactor core. It indicates that the design of the VHTR and its instrumentation placement in the RPV can help prevent air ingress. Results to date indicate that helium will, depending on the location of the break, cover the break area and prevent air ingress or at least significantly limit the air ingress due to the concentration of helium near the break. Careful placement of instrument lines in relation to the break and ventilation port can substantially limit air ingress by making sure that helium is the dominant gas near the break. Due to the thermal hydraulic calculations and comparisons in Chapter 2 suggesting that the prototype and scaled system maintain thermal hydraulic similarity, the previously stated conclusions should be considered in the VHTR design.

References

[1] K. L. Murty and I. Charit, "Structural materials for gen-iv nuclear reactors: Challenges and opportunities," *Journal of Nuclear Materials*, vol. 383, no. 1-2, pp. 189–195, 2008.

[2] D. Chapin, S. Kiffer, and J. Nestell, "The very high temperature reactor: A technical summary," MPR Associates Inc., Tech. Rep., 2004.

[3] J.-C. Gauthier, G. Brinkmann, B. Copsey, and M. Lecomte, "Antares: The htr/vhtr project at framatome anp," *Nuclear Engineering and Design*, vol. 236, pp. 526–533, 2006.

[4] "The next generation nuclear plant methods technical program plan," https://inldigitallibrary.inl.gov/sites/sti/sti/4781568.pdf (2010/12/10).

[5] "Next generation nuclear plant methods research and development technical program plan–pln-2498," Idaho National Laboratory, Argonne National Laboratory, U.S. Department of Energy, Tech. Rep., 2010.

[6] R. C. Martineau and R. A. Berry, "A preliminary investigation of rapid depressurization phenomena following a sudden dfloc in a vhtr," *Nuclear Engineering and Design*, vol. 240, pp. 1013–1021, 01 2010.

[7] T. K. Ham, D. J. Arcilesi, I. H. Kim, X. Sun, R. Christensen, and C. Oh, "On the effects of containment design to gt-mhr air-ingress accidents," *Transactions of the American Nuclear Society*, vol. 109, pp. 316–319, 11 2013.

[8] C. Oh, E. Kim, R. Schultz, M. Patterson, and D. Petti, "Thermal hydraulics of the very high temperature gas cooled reactor."

[9] E. S. Kim, C. Oh, R. Schultz, and D. Petti, "Analysis on the density driven air-ingress accident in vhtrs," *November 2008 ANS Conference Proceedings*, pp. 842–844, 11 2008.

[10] "Development of safety analysis codes and experimental validation for a very high temperature gas-cooled reactor," Idaho National Laboratory, Tech. Rep., 2006.

[11] D. Arcilesi, "Experimental verification of the initial stages of an htgr double-ended guillotine break," Ph.D. dissertation, Columbus, OH., 2018.

[12] D. Arcilesi, T. Ham, X. Sun, R. Christensen, and C. Oh, "Development of scaling analysis for air-ingress experiments for a vhtr," *Transactions of the American Nuclear Society*, vol. 105, pp. 978–989, 01 2011.

[13] U. R. Commission, "Gas turbine-modular helium reactor (gt-mhr) conceptual design description report," Tech. Rep., 1996.

[14] *University of Idaho Stainless Steel Pressure Vessel*, Buckeye Fabrication, 7, 2019, drawing Number 35326.

[15] I. ASM Aerospace Specification Metals, "Aisi type 316 stainless steel, annealed sheet," http://asm.matweb.com/search/SpecificMaterial.asp?bassnum=MQ316A, November 2020.

[16] Honeywell, "Gms-10 rvs series-oxygen sensors," https://stevenengineering.com/Tech_Support/PDFs/31HWOS.pdf (2010/05/01).

[17] O. Engineering, "Industrial air velocity transmitter," https://assets.omega.com/spec/FMA900A.pdf.

[18] TEquipment, "Kestrel 0857afde applied ballistics kestrel 5700 elite weather meter," https://www.tequipment.net/Kestrel/0857AFDE/Anemometer/Air-Flow/?gclid=

Cj0KCQjwreT8BRDTARIsAJLI0KJKlMqp416Q6Vrny0JijBWFfxveAqZXrm-jDOnCYahqiqN4looU0LcaAq4QEALw_wcB#description.

[19] O. Engineering, "High temperature compensated pressure transducer," https://assets.omega.com/pdf/test-and-measurement-equipment/pressure/pressure-transducers/PX32B1.pdf.

[20] Swagelok, "Pressure gauges industrial and process," https://www.swagelok.com/downloads/webcatalogs/EN/MS-02-170.PDF, February 2019.

[21] AdaFruit, "Stepper motor - nema-17," https://www.adafruit.com/product/324.

APPENDIX A

Analytical Solutions Script in Python

This section shows the Python script used to estimate the blowdown times and pressures for the $\frac{1}{20}$th scaled VHTR at the University of Idaho.

Listing A.1: Python Blowdown Script

```
# Calculating Mass Flow Rate
import math
import csv
from pylab import plot, show
import matplotlib.pyplot as plt

#from decimal import *

#clear all; close all;

###### Containment constants ######

#Givens
#Units are given in square brackets.
R = 2076.9; # Helium gas constant [J/Kg/K]
c_p = 5190.1; # Specific Heat capacity under constant P for He [J/Kg/K]
c_v = 3122.0; # Specific Heat capacity under constant V for He[J/Kg/K]

c_w = 500; # Specific Heat capacity for Vessel and internals [J/Kg/K]
V_w = 0.02; # Volume of vessel structure & internals [m^3]
rho_w = 8000;# density of vessel structure and internals [kg/m^3]

As= 1.413;# Total surface area [m^2]
V = 0.120;# Vessel free volume [m^3]
```

```
Po = 0;# steady stay reactor power [W]

gamma = 5.0/3; # ratio of specific heats for He [*unitless*]
T_amb = 300.0;# Ambiant or confinment Temp [K]
rho_amb = 0.13359;# ambiant He density[kg/m^3]
mu_amb = 1.96e-5;# ambiant He viscosity [kg/m/s or Pa*s]
a = math.sqrt(gamma*R*T_amb); #speed of sound at exit of pipe [m/s]
p_amb = 101325.0; #ambiant pressure [Pa]

mu_i = 3.84e-5;#initial He viscosity [Pa*s]
m_i = 0.201;# intial He Mass in vessel [kg]
p_i = 1.066e6;#1 initial vessel pressure [Pa]

Ti = 300.0; # initial helium temp [K]
To = 273.0; # absolute temp [K]
Twi = 300.0;# initial wall temp [K]
rho_i = m_i/V

eps = 4.5e-5;# pipe equivalant roughness for a new steel pipe [m]
L = 0.0127; # length of pipe [m]
d = 0.0127;# diameter of hot duct [m]
Ac = math.pi/4*(d**2);# flow area of duct [m^2]
Pw =math.pi*(d);# Wetted perimeter of duct [m]
D = 4*Ac/Pw; #hydrolic diameter [m]
K_c = 0.5;# Loss coefficent for sudden contraction [unitless]
f_g = 0.002;#friction factor guess []
alpha = 1;# kentic energy coefficents []

tol=1e-6;#tolerance
delta_t =0.001;#time step [s]
err = 1;
```

```
err1 = 1;

h = 2;# heat transfer coefficent [W/m^2/K]

T = Ti;
Ttemp = T
Tw = Twi;
Twtemp = Tw
p = p_i;
m = m_i;
rho = rho_i;
mu = mu_i;
t=0 ;
rho_avg= 0;
mu_avg = 0;
v_g = 0 ;
Re_g = 0 ;
f1 = 0 ;
f = 0 ;
v= 0;
m_dot=0 ;
Re=0 ;

#User defined
h = 2;

err = 1;
err1 = 1;

mdot_array= [0];
t_array = [0];
T_array = [Ti];
```

```
Tw_array = [Twi];
p_array = [p_i];
vg_array = [0];
v_array = [0];
m_array = [m_i];
rho_array = [rho_i];
i = 1;

#for i in range(1,n):
while (p-p_amb) >= 100:
    t = ((i-1)*delta_t);
    rho_avg = (rho + rho_amb)/2;
    mu_avg = (mu  + mu_amb)/2;

    while abs(err) >= tol:
        v_g =  math.sqrt((p  - p_amb)/(rho_avg*(alpha / 2.0 \\
        + 0.5*(K_c + f_g*L/D))));
        if v_g  >= a:
            Re_g = (rho_avg * a * D/mu_avg);
        else :
            Re_g = (rho_avg * v_g  * D/mu_avg);
        #end
        if Re_g  >= 4000:
            f1 = ( 0.184*Re_g  **(-0.2));
            while abs(err1) >=tol:
                f = ( (1/(-2*math.log(eps/D)/3.7 + \\
                2.51/(Re_g *math.sqrt(f1)))) **2);
                err1 = f1  - f ;
                f1  = f ;

            #end
        else:
```

```
            f  = 64.0/Re_g ;
    #end

    #print "t=  ", t
    v = (math.sqrt((p - p_amb)/(rho_avg *(alpha/2.0 + \\
    0.5*(K_c + f *L/D)))));
    err = abs(v_g  - v) ;
    f_g = f ;

#end
if v  >= a:
    m_dot = ( rho_avg * Ac * a);
    Re = ( rho_avg * a * D / mu_avg);
    v = a;
else :
    m_dot = ( rho_avg * Ac * v);
    Re = ( rho_avg * v * D / mu_avg);
#end
m = ( m  - m_dot  * delta_t);
T =(delta_t*h*As/(c_v * m )*Tw +(1-delta_t*(h*As+m_dot*R)/ \\
(c_v * m ))*T );
Tw =(delta_t*0.066*Po*((i)*delta_t+(delta_t**2)**(-0.2))/(rho_w * \\
V_w*c_w)+delta_t*h*As/(rho_w*V_w*c_w)*T+(1-delta_t*h*As/(rho_w*V_w\\
*c_w))*Tw);
t = ( t  + delta_t);
#Twtemp = Tw
#Ttemp = T
mu = ( 1.865e-5 * (T/To) **(0.7));
rho = ( rho  - m_dot  * delta_t/V);
p = (rho  * R * T);
#m =  p*0.12/(R*T) #Re-calculating the mass based on pressure values
#rho = p/(R*T) #Re-calculating the demsity based on pressure values
```

```
#store wanted values
t_array.append(t);
mdot_array.append(m_dot);
m_array.append(m);
T_array.append(T);
Tw_array.append(Tw);
p_array.append(p);
vg_array.append(v_g);
v_array.append(v);
rho_array.append(rho);
i = i+1;

#end
err = err + 1;
err1 += 1;
```